บทบาทของอลูเมทิลเลชั่นและการฉีกขาดของดีเอ็นเอสายคู่ที่เกิดขึ้นเองต่อการป้องกันความไม่เสถียรของจีโนม

นางสาวมธุรดา เพชรสังข์

วิทยานิพนธ์นี้เป็นส่วนหนึ่งของการศึกษาตามหลักสูตรปริญญาวิทยาศาสตรดุษฎีบัณฑิต
สาขาวิชาชีววิทยาศาสตร์ (สหสาขาวิชา)
บัณฑิตวิทยาลัย จุฬาลงกรณ์มหาวิทยาลัย
ปีการศึกษา 2559

THE ROLE OF ALU METHYLATION AND PHYSIOLOGIC-REPLICATION INDEPENDENT-ENDOGENOUS DNA DOUBLE STRAND BREAKS (PHY-RIND-EDSBs) ON GENOMIC INSTABILITY PREVENTION

Miss Maturada Patchsung

A Dissertation Submitted in Partial Fulfillment of the Requirements

for the Degree of Doctor of Philosophy Program in Biomedical Sciences

(Interdisciplinary Program)

Graduate School

Chulalongkorn University

Academic Year 2016

Thesis Title	THE ROLE OF ALU METHYLATION AND PHYSIOLOGIC-REPLICATION INDEPENDENT-ENDOGENOUS DNA DOUBLE STRAND BREAKS (PHY-RIND-EDSBs) ON GENOMIC INSTABILITY PREVENTION
By	Miss Maturada Patchsung
Field of Study	Biomedical Sciences
Thesis Advisor	Professor Apiwat Mutirangura

Accepted by the Graduate School, Chulalongkorn University in Partial Fulfillment of the Requirements for the Doctoral Degree

.....Dean of the Graduate School

(Associate Professor Sunait Chutintaranond, Ph.D.)

THESIS COMMITTEE

.....Chairman

(Assistant Professor Amornpun Sereemaspun)

.....Thesis Advisor

(Professor Apiwat Mutirangura)

.....Examiner

(Professor Piyaratana Tosukhowong)

.....Examiner

(Professor Sittisak Honsawek)

.....External Examiner

(Siwanon Jirawatnotai)

มธุรดา เพชรสังข์ : บทบาทของอลูเมทิลเลชั่นและการฉีกขาดของดีเอ็นเอสายคู่ที่เกิดขึ้นเองต่อการป้องกันความไม่เสถียรของจีโนม (THE ROLE OF ALU METHYLATION AND PHYSIOLOGIC-REPLICATION INDEPENDENT-ENDOGENOUS DNA DOUBLE STRAND BREAKS (PHY-RIND-EDSBs) ON GENOMIC INSTABILITY PREVENTION) อ.ที่ปรึกษาวิทยานิพนธ์หลัก: ศ. ดร. นพ. อภิวัฒน์ มุทิรางกูร, 75 หน้า.

ในครั้งนี้เรามุ่งศึกษาการควบคุมแบบเหนือพันธุกรรมที่เกี่ยวข้องกับความไม่เสถียรของจีโนมซึ่งเป็นภาวะที่พบได้บ่อยในการแก่ โดยเรามุ่งเน้นไปที่การควบคุมแบบเหนือพันธุกรรมสองหัวข้อหลัก ประการแรกคือการเกิดเมทิลเลชั่น (methylation) ที่ตำแหน่ง Alu (Alu element) ซึ่งเป็นตำแหน่งที่มีลำเบสซ้ำๆกันเป็นสายสั้นๆและมีการศึกษากันมากว่ามีความเชื่อมโยงกับลักษณะการแก่หลายประการ ประการที่สองคือ การฉีกขาดของดีเอ็นเอที่เกิดขึ้นเอง ที่เรียกว่า endogenous DNA double strand breaks (EDSBs) ซึ่งการเปลี่ยนแปลงภาวะสมดุลของ EDSBs เป็นหนึ่งในกลไกที่ก่อให้เกิดความไม่เสถียรของจีโนมขึ้นในเซลล์ที่ไม่มีการแบ่งตัว (non-dividing cells) แรกสุดเราพบความสัมพันธ์เชิงลบระหว่างระดับ Alu methylation ของดีเอ็นเอที่ได้จากเลือดของคนปกติและความเสียหายของดีเอ็นที่เกิดขึ้นเอง (endogenous DNA damages) เราจึงนำ siRNA ที่มีความจำเพาะกับ Alu element (siRNA-Alu) ใส่เข้าไปในเซลล์ของมนุษย์ที่มีการแบ่งตัวได้ไม่จำกัดและที่แบ่งตัวได้จำกัด เราพบว่าเซลล์ที่มีการใส่ siRNA-Alu จะมีระดับ Alu methylation เพิ่มขึ้น ซึ่งระดับเมทิลเลชั่นที่เพิ่มขึ้นนี้มีความจำเพาะที่ตำแหน่งของ Alu element เท่านั้นและพบการคงอยู่ของระดับ methylation ที่เพิ่มขึ้นในระยะเวลาหนึ่ง นอกจากนี้พบว่าการเพิ่มขึ้นของระดับ Alu methylation ขึ้นอยู่กับลักษณะการจับของ siRNA ที่ Alu element ที่สำคัญคือ เราพบว่า Alu methylation สามารถทำให้เกิดการเปลี่ยนแปลงฟีโนไทป์ของเซลล์ได้ โดยเซลล์ที่มีระดับ Alu methylation เพิ่มขึ้น จะมีการแบ่งตัวที่เร็วกว่า มีระดับ endogenous DNA damage ที่ต่ำกว่า แต่สามารถทนต่อสารที่ทำร้ายดีเอ็นเอได้ดีว่าเซลล์ในกลุ่มควบคุม ดังนั้นเราจึงเสนอว่า siRNA-Alu ที่ส่งเสริมให้เกิด Alu methylation เป็นเครื่องมือหนึ่งที่มีประสิทธิภาพในการใช้ป้องการความไม่เสถียรของจีโนม ในทำนองเดียวกันในสภาพปกติ เซลล์ยูคาริโอต จะลดความดึงเครียดของจีโนมโดยการเก็บรักษา EDSBs ชนิดหนึ่งเอาไว้ เราเรียก EDSBs ชนิดนี้ว่า physiologic replication independent EDSBs (phy-RIND-EDSBs) ในการศึกษานี้มีการใช้เทคนิคพีซีอาร์และวิเคราะห์ลำดับเบสของดีเอ็นเอเพื่อวิเคราะห์ปริมาณและจัดกลุ่ม RIND-EDSBs เพื่อหากลไกการเกิดความไม่เสถียรของจีโนมที่ก่อให้เกิดการแก่ในเซลล์ที่ไม่มีการแบ่งตัว ผลการวิเคราะห์พบว่าเซลล์แก่จะมีระดับ phy-RIND-EDSBs ลดลง มีข้อบกพร่องในการซ่อมแซม DSBs (DSB repair) และมีการสร้าง pathologic RIND-EDSBs (path-RIND-EDSBs) เพิ่มขึ้น โดย path-RIND-EDSBs สามารถเกิดขึ้นได้เองและกระตุ้นการซ่อมแซม EDSBs ซึ่งรวมถึง phy-RIND-EDSBs ด้วย ทำให้ระดับ phy-RIND-EDSBs ลดลง ซึ่งการลดลงของ phy-RIND-EDSBs นี้จะทำให้เกิดการสร้าง path-RIND-EDSBs เพิ่มมากขึ้น นอกจากนี้ถ้ามีการรดลงของ phy-RIND-EDSBs ร่วมกับการมีข้อบกพร่องในการซ่อมแซม DSBs จะส่งผลให้อัตราการรอดชีวิตของเซลล์ที่มีแก่แบบไม่มีการสร้างดีเอ็นเอ (chronological aging) ลดลง ผลการศึกษาเหล่านี้ชี้ให้เห็นว่า phy-RIND-EDSBs มีบทบาทเป็นการควบคุมแบบเหนือพันธุกรรมในการป้องกันความไม่เสถียรของจีโนมที่เกิดขึ้นจากการสร้าง path-RIND-EDSBs กล่าวโดยสรุป Alu methylation และ phy-RIND-EDSBs อาจใช้เป็นเป้าหมายสำคัญในการลดความไม่เสถียรของจีโนมเพื่อป้องกันการแก่ของเซลล์ได้

สาขาวิชา ชีวเวชศาสตร์ ลายมือชื่อนิสิต .....

ปีการศึกษา 2559 ลายมือชื่อ อ.ที่ปรึกษาหลัก .....

5587830820 : MAJOR BIOMEDICAL SCIENCES
KEYWORDS: ALU METHYLATION / GENOMIC INST / ENDOGENOUS DNA DAMAGE / ENDOGENOUS DNA DOUBLE STRAND BREAK

MATURADA PATCHSUNG: THE ROLE OF ALU METHYLATION AND PHYSIOLOGIC-REPLICATION INDEPENDENT-ENDOGENOUS DNA DOUBLE STRAND BREAKS (PHY-RIND-EDSBs) ON GENOMIC INSTABILITY PREVENTION. ADVISOR: PROF. APIWAT MUTIRANGURA, 75 pp.

Here, we aimed to study the epigenetic marks involving genomic instability, a common event in aging. We focused on two epigenetic marks. First is methylation of Alu element, commonly studied IRS which was proposed to associate with aging characteristics. Second is endogenous DNA double strand breaks (EDSBs), which one of the genomic instability mechanisms in non-dividing cells, change in homeostasis during aging. First, a negative correlation between the methylation of Alu in the blood-derived DNA and endogenous DNA damages was found in healthy people. Then we used siRNA-Alu to direct Alu element in human immortalized cell lines and human diploid fibroblasts. Increase in Alu methylation level was observed in cells with siRNA-Alu transfection. The de novo methylation induced by siRNA-Alu was sequence specific and sustainable. Moreover, the Increasing level of Alu methylation induced by siRNA-Alu depended on siRNA binding sites having insertion or deletion and percent identity value. Interestingly, Alu methylation altered celluar phenotypes. Hypermethylated Alu cells proliferated faster than control cells, lower endogenous DNA damages and more resist to DNA damage agents. Therefore, we proposed that siRNA-Alu promoting Alu methylation has high potential to prevent genomic instability. In the same way, in regular physiologic condition, a eukaryote relieves tension of the genome by maintaining a different kind of EDSBs, called physiologic replication independent EDSBs (phy-RIND-EDSBs). In this study, genome-wide EDSB PCR and high throughput sequencing were used to quantify sequence and classify RIND-EDSBs to explore a mechanism of how genomic instability occurs and induces senescence in non-dividing cells. We discovered a reduction of phy-RIND-EDSBs, DSB repair defect and production and retention of pathologic RIND-EDSBs (path-RIND-EDSBs) in aging cells. Path-RIND-EDSBs can occur spontaneously, and they induce the global repair of EDSBs, including phy-RIND-EDSBs. Alternately, lowered numbers of phy-RIND-EDSBs increase a generation of path-RIND-EDSBs. Accompany with DSB repair defects, path-RIND-EDSBs are retained and reduce viability in chronologically aging cells. These evidences indicated that phy-RIND-EDSBs play an epigenetic role in preventing genomic instability due to the generation and retention of path-RIND-EDSBs. As a result, taken together, Alu methylation and phy-RIND-EDSB may be used as a target to reduce genomic instability to prevent celluar aging.

Field of Study: Biomedical Sciences Student's Signature .....

Academic Year: 2016 Advisor's Signature .....

ACKNOWLEDGEMENTS

I would like to express my appreciation and sincere thanks to my thesis advisor, Professor Dr. Apiwat Mutirangura for his invaluable help, excellent advice and constant encouragement throughout the course of this research. I am most grateful for his teaching and advice, not only the research methodologies but also many methodologies on life. In addition, I am extremely grateful to Dr. Monnat Pongpanich for helpful suggestions and insightful comments during my study. I want to thank my other committees and special members. I also appreciate, Dr. Jirapan Thongsroy, Mr. Prakasit Rattanatanyong and Associate Professor Nakarin Kitkumthorn for their assistance and encouragement, this work would not have been accomplished without them. Finally, I would like to express my deepest gratitude to my family for their love and understanding all the time. This thesis was partially supported by Chulalongkorn University under the office of the Higher Education Commission.

CONTENTS

Page

THAI ABSTRACT iv

ENGLISH ABSTRACT v

ACKNOWLEDGEMENTS vi

CONTENTS vii

LIST OF FIGURES 1

CHAPTER I INTRODUCTION 1

CHAPTER II LITERATURE REVIEW 10

CHAPTER III MATERIALS AND METHODS 22

CHAPTER IV RESULTS 35

CHAPTER V DISCUSSION 60

REFERENCES 67

VITA 75

LIST OF FIGURES

Figure 1 The hallmarks of aging.. 11

Figure 2 Structure of Alu elements..... 12

Figure 3 Epigenetic changes in aging.. 14

Figure 4 Mechanism of gene silencing.. 15

Figure 5 Structure of siRNA molecule.. 16

Figure 6 Two generally used aging models in yeast.. 17

Figure 7 Yeast Chronological Life Span Major Regulatory Pathway.. 19

Figure 8 The methylation patterns of Alu detected by COBRA-Alu.. 24

Figure 9 Work flow of Alu methylation Ion torrent data and analysis.. 26

Figure 10 Schematic representation of RIND-EDSB-detection. 30

Figure 11 Work flow of Linker-mediated Ion torrent data processing and analysis.. 33

Figure 12 A univariate correlation analysis 36

Figure 13 Percentage of Alu methylation level in cells transfected with siRNA-Alu. 38

Figure 14 The percentage of Alu methylation levels of each position 39

Figure 15 The percentage of LINE1 methylation levels of cells with siRNA-Alu transfection.. 40

Figure 16 The percentage of Alu methylation at day 2 and day 7. 40

Figure 17 Alu methylation of each allele using high-throughput sequencing..... 42

Figure 18 The percentage of Alu methylation level in periodontal ligament (PDL) fibroblast. 43

Figure 19 Proliferation in siRNA-Alu transfected cells.. 44

Figure 20 Hypermethylated Alu cells had a decreased sensitivity to DNA damage agent.. 46

Figure 21 A comparison of 8-OHdG and AP site level in HEK293 cells between control and siRNA-Alu transfected cells.. 47

Figure 22 RIND-EDSBs and sequences in chronologically aging yeast.. 49

Figure 23 sequence of caffeine treatment in JKM179 yeast strains.. 52

Figure 24 Percent viability on days 0-30 following HO induction. A break was induced every ten days in old culture of JKM179 by HO induction. 52

Figure 25 RIND-EDSBs and sequences in HO induction. 54

Figure 26 Sequence of caffeine treatment in HO induction.. 56

Figure 27 Sequence of nhp6a deletion yeast strains (*nhp6aΔ*).. 58

Figure 28 Schematic representation of how RIND-EDSBs reduce cell viability during the yeast life cycle. 65

CHAPTER I
INTRODUCTION

Background and rationale

Genomic instability is a precursor to mutation leading to cellular aging and cell death (*1-3*). Global hypomethylation during aging process is related to demethylation of DNA repetitive elements (*4-7*). Interspersed repetitive sequences (IRS) are a main contributor to genome size (~45%) (*8, 9*). Therefore, loss of IRS methylation was believed to be the major contributor of global hypomethylation. IRS comprises of short interspersed elements (SINEs), long interspersed elements (LINEs), long terminal repeat (LTR)-retrotransposons and DNA transposons. Alu is the most abundant SINE. Recently, an experimental study found a significant association between age and Alu hypomethylation but this association was not found in LINE1 hypomethylation (*10*). Further evidence confirming this finding obtained in volunteers with age between 20-88 years that age was negatively associated with Alu methylation levels but not LINE-1 (*11*). Moreover, there are positive correlations between Alu hypomethylation in blood cells and many age-related phenotypes (*12*). As a result, in this study we focus on the role of Alu methylation on genomic instability. We address the question that how to restore the Alu methylation to reduce genomic instability and prevent cellular aging. It has recently been show that both synthetic and expressed short interfering RNAs (siRNAs) and short hairpin RNAs (shRNAs), mention as RNA directed DNA methylation (RdDM) were able to generate DNA methylation in human cells (*13, 14*). So if we can prevent loss of Alu methylation using RdDM function, we may be also to prevent genomic instability and aging.

Another important molecular mechanism underlying genomic instability is DNA double strand breaks (DSBs) and DSB repair. In our previous work, we discovered that there are two distinct types of Endogenous DNA Double strand break (EDSBs) in non-replicative cells. The first type is pathologic DNA lesions, pathologic-EDSBs. Pathologic-

EDSBs, like the replication or irradiation induced DSBs (*15*), lead to mutations and induce cell death (*16, 17*). These EDSBs are quickly repaired and are detectable directly only when inhibit DSB repair process (*16*). Whereas, the other, physiologic-EDSBs, without DSB repair inhibition, is detectable in yeast and all human cell types, not related to **Δ**-H2AX, and retained in heterochromatin. Physiologic-EDSBs are located non-randomly. Most of physiologic-EDSBs are resided within hypermethylated genome (*18*) and occurred right after "ACGT" sequence (*19*). Physiologic-EDSBs may play an important role in prevent genomic instability.

I. Alu methylation and genomic instability

Commonly studied interspersed repetitive sequences (IRSs) include Alu elements, long interspersed element-1 (LINE-1), and human endogenous retrovirus (HERV) (*11*). Alu belong to the SINE family (Short Interspersed Nuclear Elements) of repetitive elements. There are over one million Alu elements in the human genome (*20, 21*). Alu elements, as well as other repetitive elements, were at previous considered as junk DNA but recently studies show that the presence of Alu elements had a great effect on the human genome. Alu hypomethylation was found in several diseases and morbidity conditions including cancer cells (*22-24*), white blood cells of aging people (*10, 11*), people who smoked (*25*) and osteoporosis patients (*12*).

A progressive loss of DNA methylation during the aging process is associated with demethylation of those DNA repetitive elements. In aging, Bollati et al. (2009) found that Alu methylation was negatively associated with age at the visit of subjects. A poor association was observed with LINE-1 elements. They also observed a significant decrease in average Alu methylation over time. Interestingly, the longitudinal decline in Alu methylation was linear and highly correlated with time since the first measurement. In contrast, average LINE-1 did not vary over time (*10*). These findings were confirmed in later studies by Jintaridth and Mutirangura who found that age was negatively associated with methylation levels of Alu but not LINE-1. Loss of methylation of Alu occurred during age 34-68 year (*11*). According to the study of Jintaridth et al. (2013) in

post-menopausal women, there were positive correlations between Alu hypomethylation in blood cells and several age-related phenotypes in bone and body fat (*12*). Therefore, These finding leading to suggest that not only the biological causes and consequences of genomic hypomethylation but also the role of repetitive elements especially Alu in the aging process.

The consequences of interspersed repetitive sequence hypomethylation include gene expression change and genomic instability. DNA hypomethylation in LINE-1 and HERV were reported to possess gene regulatory functions but not Alu. Therefore, Alu elements are the most appropriate targets for a genomic instability study.

II. Physiologic-replication independent endogenous DNA double strand breaks (phy-RIND-EDSBs) and genomic instability

In our previous work, we discovered endogenous DNA double strand breaks (EDSBs) that occurred in non-replicating cells without using any inducing agents, named replication independent EDSBs (RIND-EDSBs) (*16, 18*). The causes and consequences of RIND-EDSBs were different from DSBs with occur by replication or irradiation. Whereas, irradiation-induced DSBs suspend cell cycle, causing mutations, and induce cell death (*26*), RIND-EDSBs did not injure the cell. In conclusion, RIND-EDSBs are not only ubiquitously expressed in human cells. Therefore, we postulated that RIND-EDSBs have and important function and occur non-randomly. Characteristics of RIND-EDSBs were determined and we found that breaks scattered along the chromosomes and the number of breaks positively correlated with chromosome size. Most importantly, breaks occurred most frequently after “ACGT” drew some attention to the “ACGT” pattern itself (*19*). In addition, RIND-EDSBs were more likely retained in heterochromatin. Since heterochromatin typically occurred at CpG sites, this could be connected to having “ACGT” pattern at breaks. The specificity of “ACGT” was not a coincidence either, as adenine and thymine was more abundance than cytosine and guanine in the yeast genome. This suggested that the productions of RIND-EDSBs are results of specific mechanisms. The mechanism could resemble how restriction

enzymes recognize specific nucleotide sequences. It was unlikely that mechanism was chromosome location dependent since we observed break locations scattered along chromosome suggesting distinct RIND-EDSBs locations in each cell. Although, the mechanism is still unknown, we hypothesize that there is specific mechanism for RIND-EDSBs occurrences. Since RIND-EDSBs are conserved from yeast to human, the RIND-EDSBs producing mechanism should playing important role in preventing genomic instability.

III. Concluding hypothesis

We hypothesized that the human genome may use DNA methylation in IRS to prevent genomic instability. This molecular event is commonly found in aging and cancer cells (*10-12, 22*).Therefore, a tool to prevent genomic instability may be useful in prevention of diseases such as cancer and morbidity conditions in the aging process. Alu elements are the most appropriate targets for a genomic instability study. There are over one million Alu elements in the human genome. Alu hypomethylation was found in several diseases and morbidity conditions including cancer cells (*22-24*), white blood cells of aging people (*10, 11*), people who smoked (*25*) and osteoporosis patients (*12*). Finally, DNA methylation in LINE-1 and HERV were reported to possess gene regulatory functions (*27-29*). Therefore, increasing LINE-1 or HERV methylation may cause other effects in addition to genomic instability reduction.

By observing cell survival from vanillin, a DNA-PKCs inhibitor, we found that the cell possessed more retained RIND-EDSBs survived more than the others (Dr. Araya, unpublished data). Therefore, the retention of RIND-EDSBs in heterochromatin may be epigenetic mark that may play an important role to prevent genomic instability and celluar aging. To further investigate the role of RIND-EDSBs in aging, we chose to use yeast as a model system. Yeast has proved to be applicable to higher organism.

Thus, the main objective of this project is to investigate if Alu methylation and RIND-EDSBs are epigenetic marks that play a role in preventing genomic instability and

celluar aging. So, genomic instability may cause aging via reduction of Alu methylation and RIND-EDSBs.

Research questions

1. Does siRNA-Alu can increase Alu methylation level?

2. Does Alu methylation can prevent genomic instability?

3. How are levels and characteristics of RIND-EDSB sequences in chronological yeast?

4. How are RIND-EDSBs effect genomic instability and promote aging in non-dividing yeast cells?

Hypotheses

1. siRNA-Alu can increase Alu methylation level.

2. Alu methylation would prevent genomic instability.

3. The levels and characteristics of RIND-EDSB sequences would be change in chronological aging.

4. Altered RIND-EDSB sequences in aging cells should lead to change other EDSBs

Objectives

1. To examine if siRNA-Alu can increase Alu methylation level.

2. To examine if Alu methylation can prevent genomic instability.

3. To quantify sequence and classify RIND-EDSBs in chronological aging yeast.

4. To establish how RIND-EDSB sequence associated with genomic instability and promote aging in non-dividing cells.

Conceptual framework

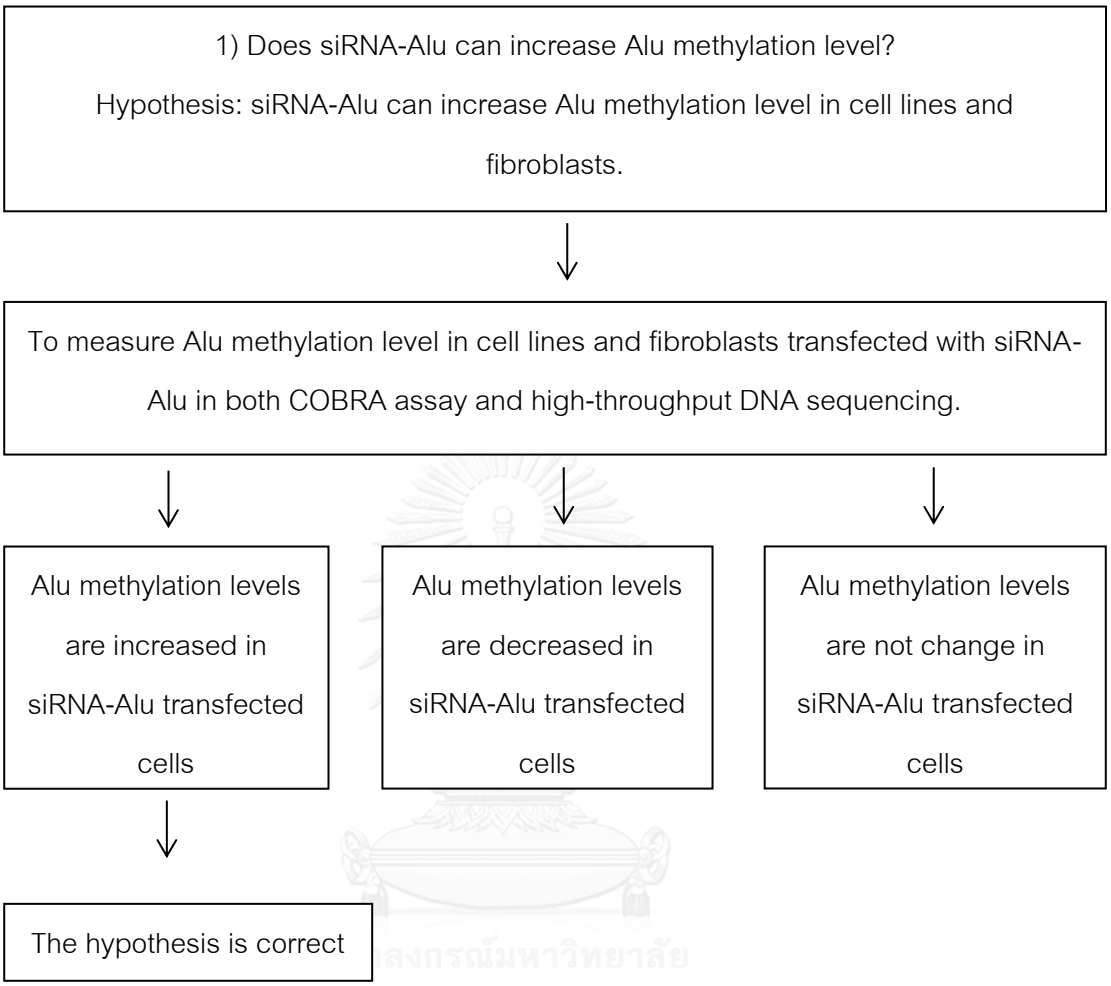

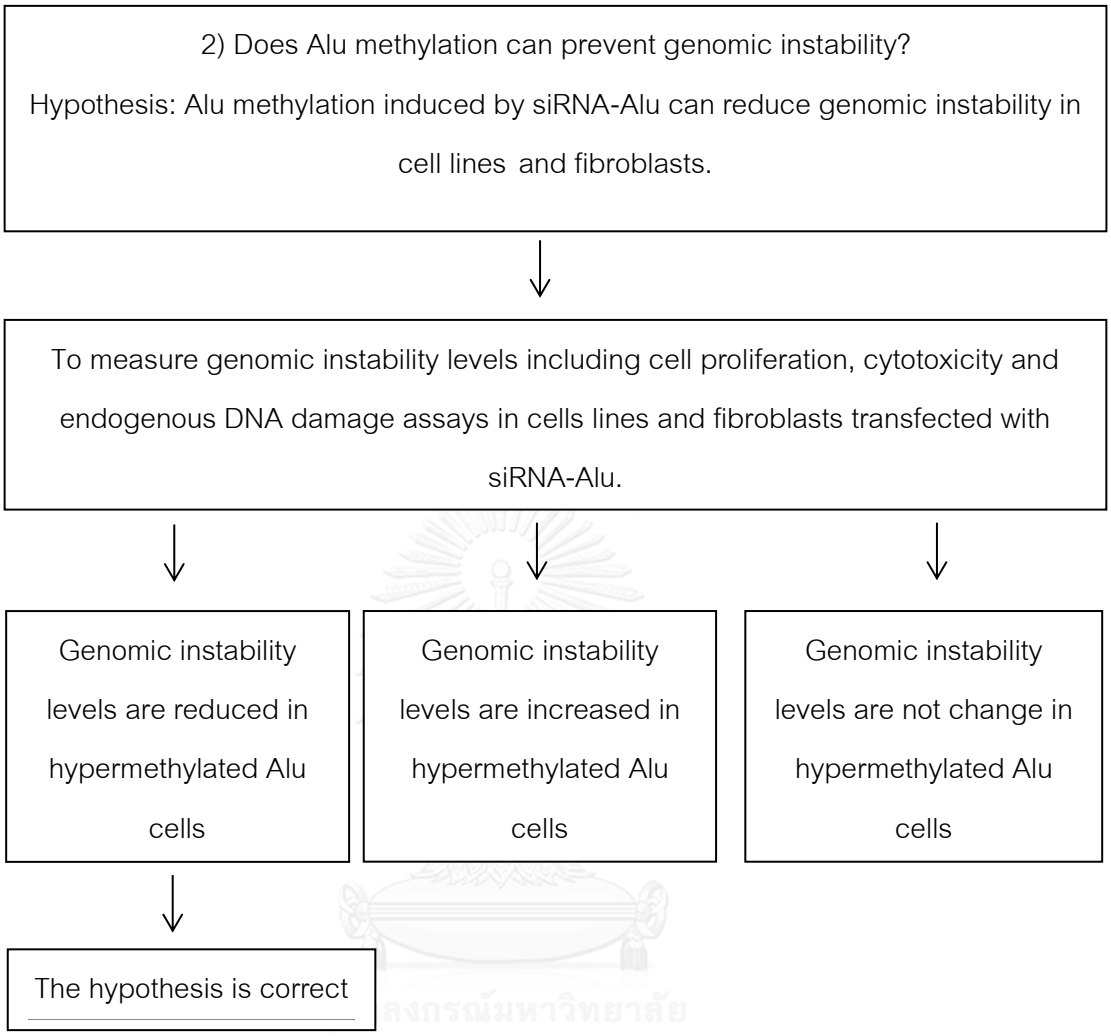

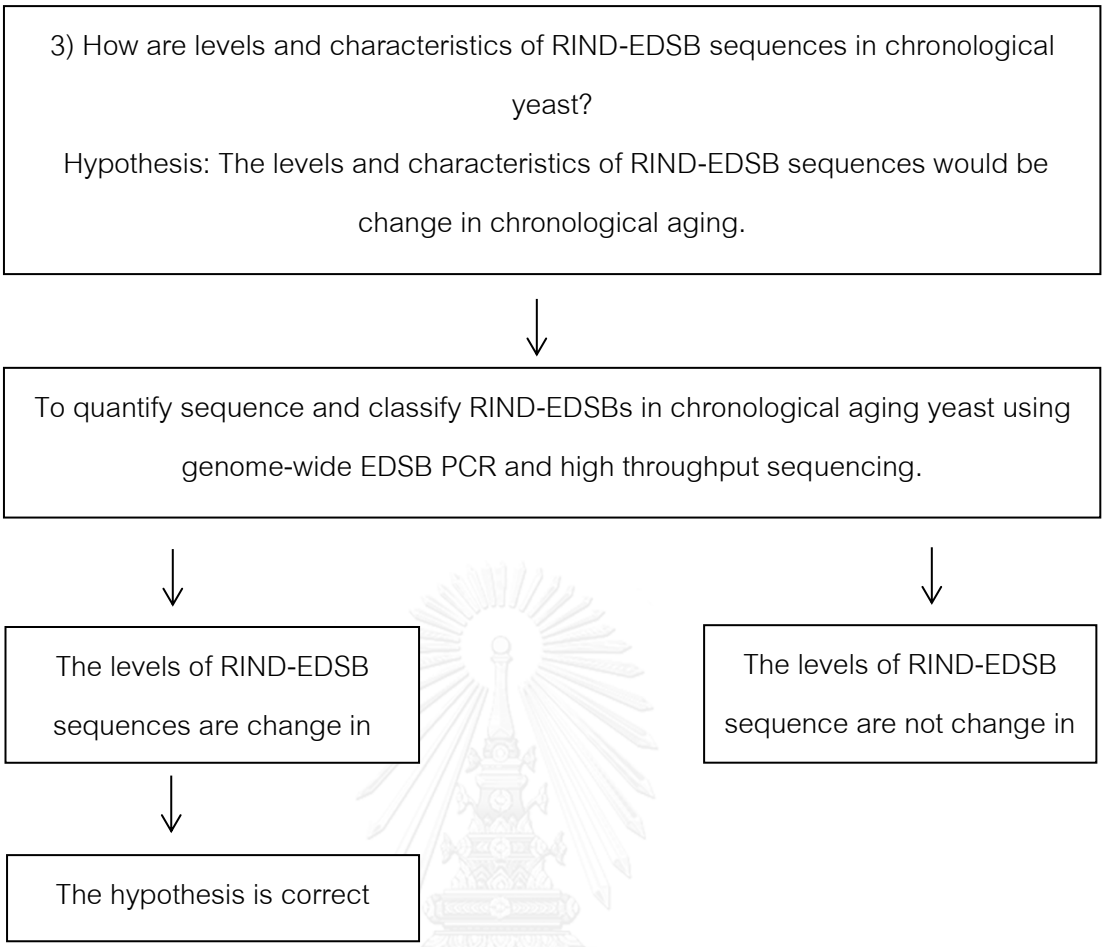

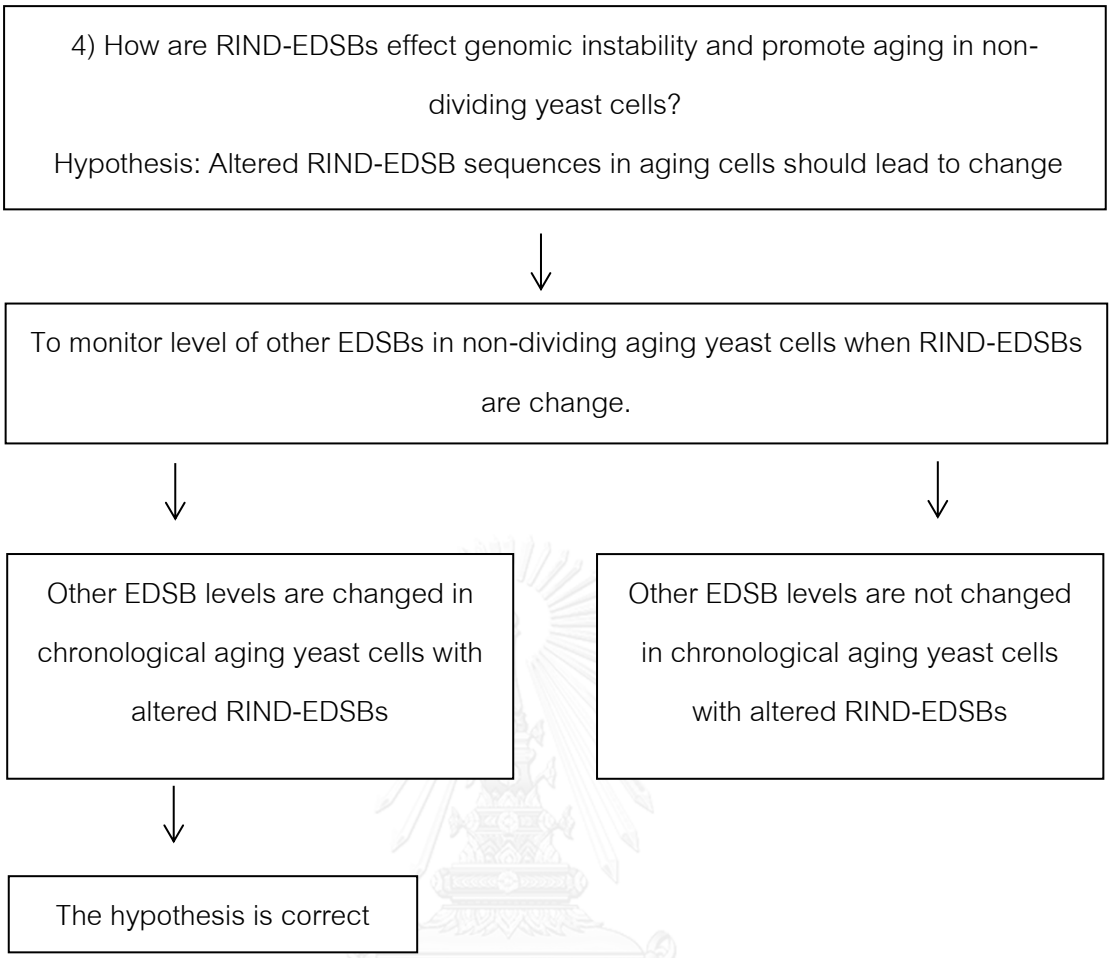

CHAPTER II
LITERATURE REVIEW

Cellular aging

Aging can be considered as a progressive loss of physiological integrity, leading to defective function and increase exposed to the risk of being attacked or harm to death. This state or process of being or becoming degenerate is the risk factor for major human pathologies including cancer, diabetes, cardiovascular disorders and neurodegenerative disease (*30*).

There are nine candidate hallmarks that are considered to contribute to the aging process and together define the aging phenotype. These hallmarks are genomic instability, telomere attrition, epigenetic alteration, loss of proteostasis, deregulated nutrient sensing, mitochondrial dysfunction, cellular senescence, stem cell exhaustion, and alter intercellular communication (Figure 1) (*30*) . Defining hallmarks of aging may contribute to construct a framework for future studies on molecular mechanisms of aging and designing interventions to enhance human life span.

Figure 1 The hallmarks of aging. The nine hallmarks of aging include genomic instability, telomere attrition, epigenetic alterations, loss of proteostasis, deregulated nutrient sensing, mitochondrial dysfunction, cellular senescence, stem cell exhaustion, and altered intercellular communication (*30*).

Alu elements

Fifty-five percent of human genome is composed of repetitive elements (*31*). Among different families of interspersed repetitive sequence (IRS), Alu elements are the most abundant IRS in the human genome. They are present in more than one million copies or 10% of the human genome. Alu belong to the SINE family (Short Interspersed Nuclear Elements) of IRS. Modern Alu elements are 300 bp in length. Their amplification has been dependent on the transposition machinery of other retrotransposons, since they do not encode any protein. It has recently been shown that they could use LINE-1 (long interspersed nuclear elements) elements for this purpose (*32*). Alu elements, as well as other IRS, were previously considered as junk DNA but recent studies state that the presence of Alu elements had a great effect on the human genome in both negative and positive (*33*).

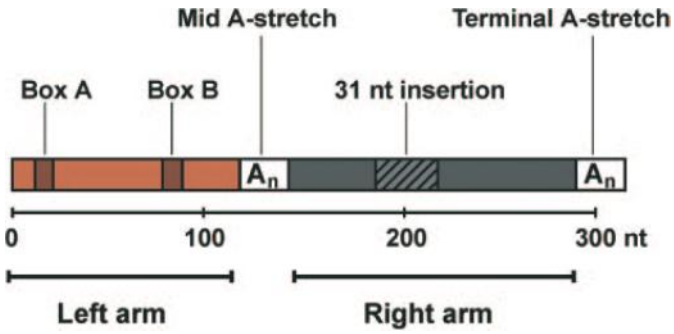

Figure 2 Structure of Alu elements. Alu elements are about 300 nucleotide (nt) long; they have a dimeric structure comprised of two related but not equivalent monomers (left and right arms). The right arm consists of a 31 nt insertion as compared to the left arm. Left and right arms located separately by an A-rich region (Mid A-stretch) and followed by a short poly (A) tail (Terminal A-stretch). The left arm consists of functional, but weak, A and B boxes of the RNA polymerase III internal promoter.

Alu methylation and aging

In aging, Bollati et al. (2009) found that Alu methylation was negatively associated with age at the visit of subjects ($b = -0.12$, $p = 0.0005$). A weaker association was observed with LINE-1 elements ($b = -0.06$, $p = 0.049$). They also observed a significant decrease in average Alu methylation over time, with a -0.2 %5 mC change ($p = 0.012$) compared to blood samples collected up to 8 years earlier. Interestingly, the longitudinal decline in Alu methylation was linear and highly correlated with time since the first measurement ($b = -0.089$, $p < 0.0001$). In contrast, average LINE-1 did not vary over time (*10*). These findings were confirmed in later studies by Jintaridth and Mutirangura who found that age was negatively associated with methylation levels of Alu ($r = -0.452$, $p < 0.01$) but not LINE-1 ($r = 0.145$, $p = 0.055$). Loss of methylation of Alu occurred during age 34-68 years (*11*) . According to the study of Jintaridth et al. (2013) in post-menopausal women, there were positive correlations between Alu hypomethylation in blood cells and several age-related phenotypes in bone and body fat (*12*). Therefore, These finding leading to suggest that not only the biological causes

and consequences of genomic hypomethylation but also the role of repetitive elements especially Alu in the aging process .

Aging and genomic hypomethylation

The hallmarks of aging may be useful to the future studies on molecular mechanisms of aging leading to increase human life span. One interesting of nine hallmarks of aging is epigenetic alteration changes particularly changes in DNA methylation that can cause cell instability that lead to the aging process (Figure 3) (*30*). The precise status of DNA methylation is balanced in mature cell but this balance in aging cells is strongly moved to DNA hypomethylation. DNA demethylation could also have an influence on aging cells. The first evidence of the age dependent loss of genome methylation found that during humpback salmon life span, the amount of 5-methylcytosine (5meC) in isolated DNA was decrease. This finding was supported by later studies that age-dependent DNA methylation was found in many mammalian tissue, embryonic tissue, and new born animals were gradually the amount of 5meC in DNA isolated from aging cells are decrease. Vanyshin *et al*. noted that human fibroblasts treated with demethylating agent 5-aza-2'-deoxycytidine (5-aza-dC) to induce DNA demethylation showed a considerably shortened life span. An aging process was primarily associated with demethylated DNA leading to genomic instability (*34*).

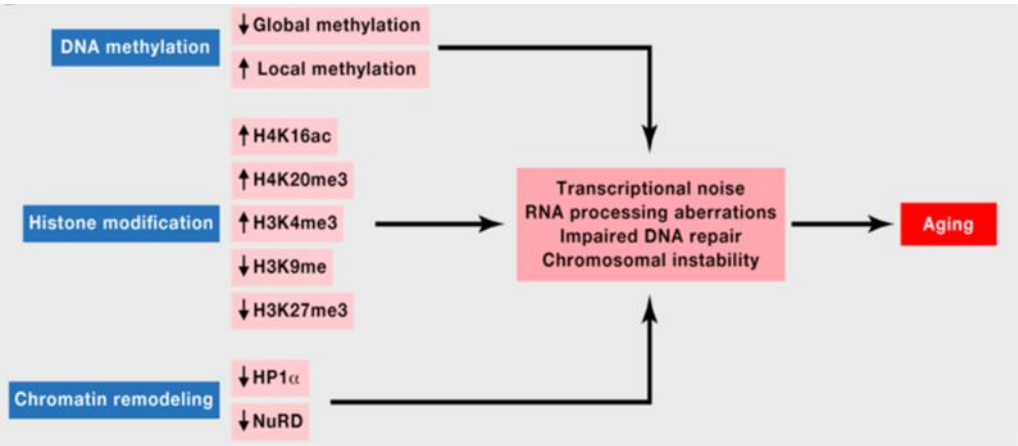

Figure 3 Epigenetic changes in aging. Changes in the DNA methylation or acetylation and histone methylation, as well as of other chromatin-associated proteins, can induce epigenetic alterations that lead to the aging process (*30*).

RNA directed DNA methylation (RdDM)

RNA interference or RNAi is a post-transcriptional gene regulation in which causes RNA degradation of complementary RNA sequences. Moreover, siRNAs can participate into another pathway by which a different argonaute-family protein leads to inhibit beginning transcripts that are still bind to RNA polymerase II and the DNA strand. This alternative pathway occurs in nucleus on area of chromatin for modification by the induction of protein complexes to incorporate the methylation of the histone and cytosine bases of DNA. This modification contributes to condensed and unavailable for transcription (Figure 4) (*35*).

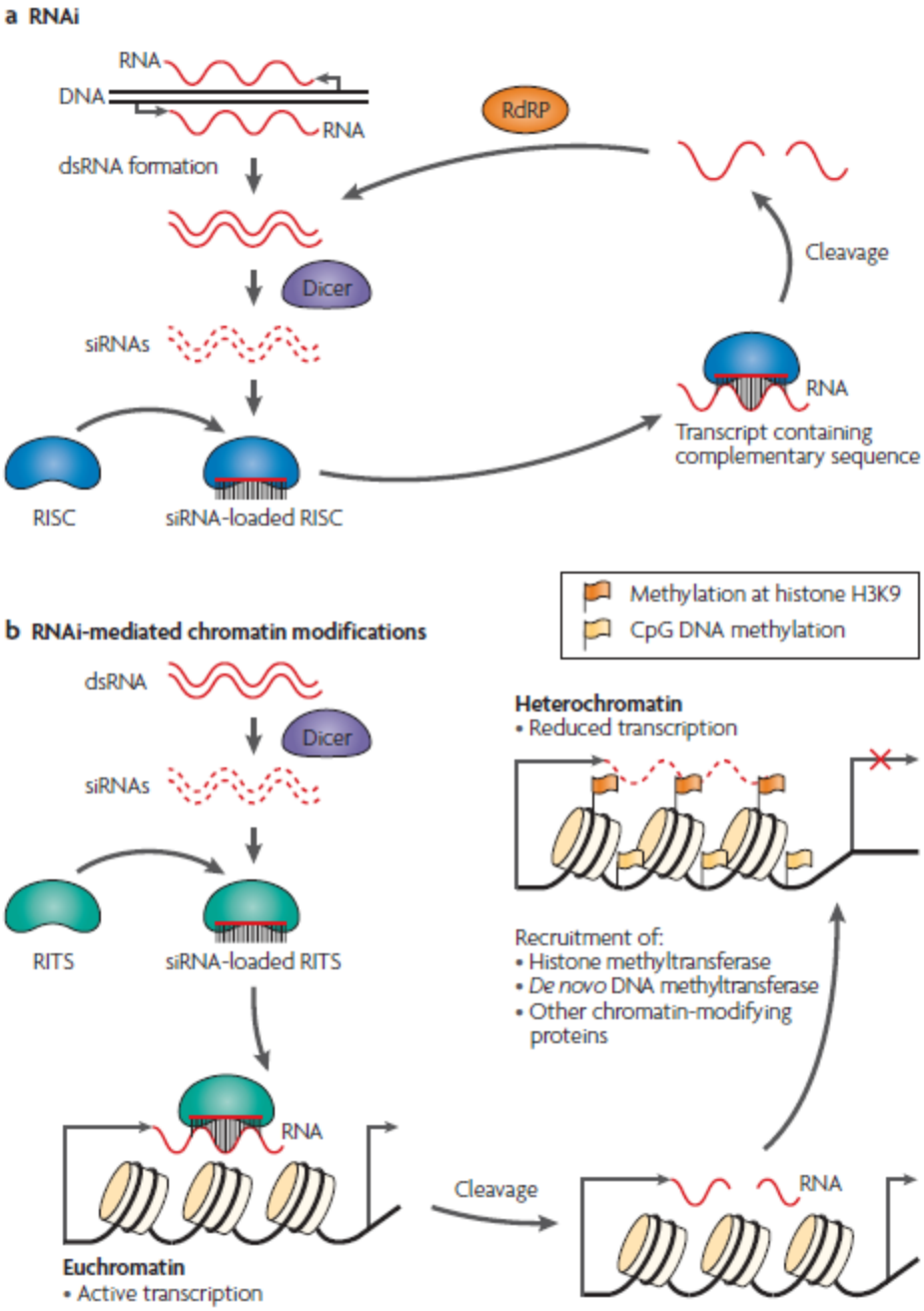

Figure 4 Mechanism of gene silencing. (A) Role of RNAi pathway in post transcriptional regulation leading to RNA degradation. (B) RNAi induces chromatin and DNA modification leading to inaccessibility to transcription (*35*).

Structure of siRNA is shown in figure 5. Each strand has a 5' phosphate group and a 3' hydroxyl (-OH) group. This structure is the result of processing by Dicer, an enzyme that converts either long dsRNAs or hairpin RNAs into siRNAs. SiRNAs can also be exogenously (artificially) introduced into cells by various transfection methods to bring about the specific knockdown of a gene of interest. Essentially any gene of which the sequence is known can thus be targeted based on sequence complementarity with an appropriately tailored siRNA.

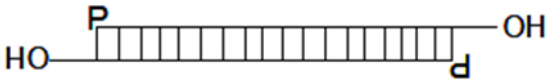

Figure 5 Structure of siRNA molecule. A ~ 19-21 base pairs RNA core duplex that is followed by a 2 nucleotide 3' overhang on each strand.

RdDM was first detected in a viroid system in plants by Wassenegger who proposed that RNA-DNA interactions can act as a signal that triggers de novo DNA methylation in plants (*36*). There was a suggestion that viroids and/or their replication intermediates are directly associated with inducing methylation of the homologous DNA. Following virus infection, nuclear transgenes homologous to viral sequences became methylated, indicating that viral RNAs present in the cytoplasm entered the nucleus and triggered DNA methylation. Further evidence confirming these results showed that siRNA generated in plant consists of short (21-22 nt) and long (24-26 nt) size classes, whereas those from endogenous retroelements are only in the long class. These classes of siRNA have different effects. The long siRNA associated with systemic silencing and methylation of homologous DNA. In contrast, short siRNA class correlated with mRNA degradation but not with systemic signaling or methylation (*37*). Moreover, Chan et al. found that defected in an siRNA-metabolizing pathway failed to induce DNA methylation of FWA transgenes (*38*). Furthermore, the study in human cells demonstrated that short hairpin RNAs (shRNAs) complementary to the RASSF1A promoter can induce low levels of de novo DNA methylation and partial gene silencing in HeLa cells (*13*).

Therefore, the involvement of dsRNA in directing DNA methylation would indicate that this molecule plays a role not only in cytoplasm to initiate the RNA degradation step of post transcriptional gene regulation but also at the genome level to induce epigenetic modifications.

Aging in yeast

The budding yeast *Saccharomyces cerevisiae* can be further considered a preeminent model for aging studies. Furthermore, the aging process of yeast cells is conserved with multicellular eukaryotes. Thus, yeast is use widely as a model organism in aging study. Cellular aging in yeast can be classified into two classed as replicative life span (RLS) and chronological life span (CLS). The replicative life span is measured by the number of times that daughter cells can divide from the mother cell till cell division stop, whereas chronological life span is measured by the length time non-dividing yeast cells can survive (figure 6) (*39*).

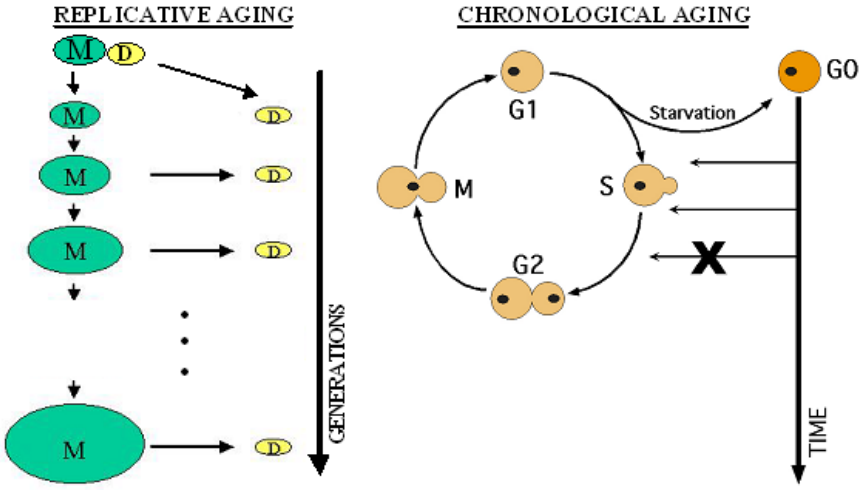

Figure 6 Two generally used aging models in yeast. In the replicative aging assay, the metric of aging is the number of daughter cells that one mother can produce, which is equivalent to the number of mitotic divisions. In the chronological assay, aging is measured as the time in stationary phase that a cell can maintain viability as defined by its ability to proliferate when restored to rich media (*39*).

Chronological life span

Chronological life span (CLS) is currently used in several laboratories worldwide (*40*). *Saccharomyces cerevisiae* is a simple model to study chronological aging. CLS is typically measured as survival of non-dividing cells. Generally is cell stop dividing within 2-7 days after starting culture and viability of cell is monitored by colony forming units (CFUs) (*41*). Yeast enters stationary phase when nutrient is limited, several proteins were discovered playing a role in life span regulation. Various studies in genetic utilizing, nutrient-sensing, and mitochondria respiration have indicated that many pathways are worded in the mechanism of chronological aging. The yeast model has been successful to identify genes which implicated to control life span.

Two major pathways regulating CLS in yeast are PKA and Tor/Sch9 pathway (Figure 7). These pathways concentrate on transcription factors that mediate the expression of stress-responsive genes (*39, 40, 42*). In addition, interestingly, yeast CLS extension is associated with a reduction in genomic stability (*43-45*). Different types of age-dependent DNA mutations were accumulated including base substitutions, small DNA insertion/deletions, and gross chromosomal rearrangements (*46*). A reduction of this effect is observed in mutant lacking Sch9 (*43-45*). In addition, many studies suggested that Sch9 implicates genomic instability in aging yeast in terms of: (1) down-regulating the expression of anti-oxidant genes, which increases DNA oxidation, (2) activating error-prone repair systems which increases mutations, (3) generating an accumulation of ethanol and acetic acid that promotes acidification (*47*).

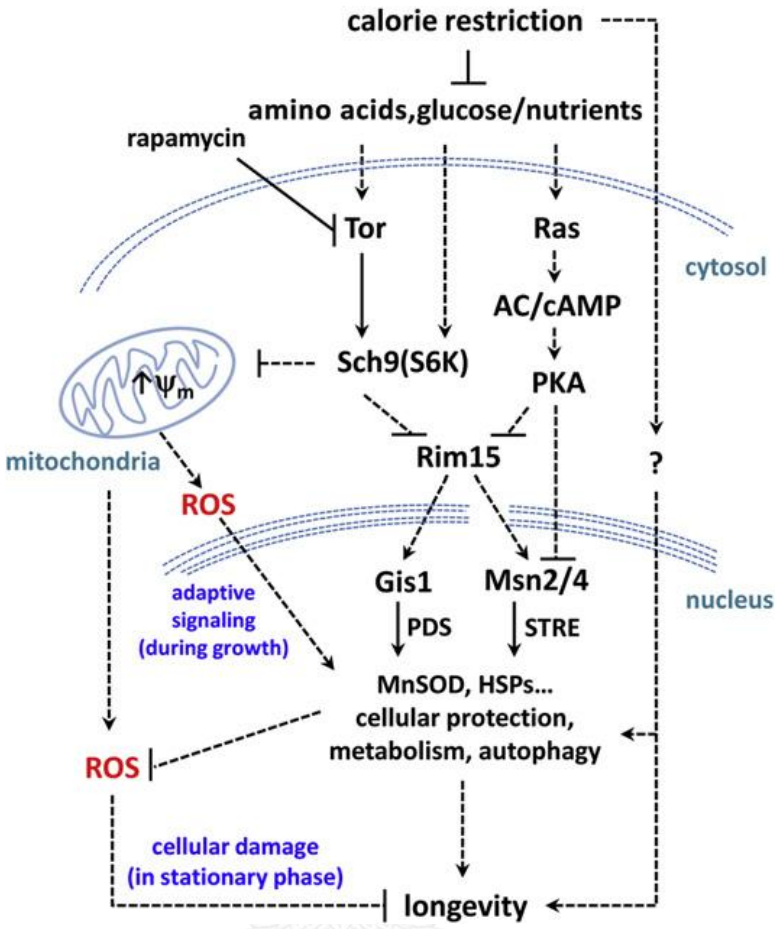

Figure 7 Yeast Chronological Life Span Major Regulatory Pathway. Sch9, Tor, and Ras eventually activate the protein kinase Rim15 to control nutrient-sensing pathway. The down-stream are activated by the Rim15-controlled Msn2/4 and Gis1 stress-responsive transcription factors (*39*).

Replication independent endogenous DNA double strand breaks (RIND-EDSBs)

DNA damage can occur by environmental factors such as chemicals, radiation or ultraviolet light. Moreover, DNA damage is induced by some mistakes inside the cell during DNA replication or normal cellular metabolism. One principally harmful form of DNA is double strand breaks (DSBs). DSBs can easily lead to gross chromosomal aberrations if not rejoined quickly. Even if it is repaired, the repair process may be error-prone, and may eventually be harmful to the organism. The process of DSB repair is also influenced by histone modification. In eukaryotic cells, a modification that occurs specifically at the location DSBs is phosphorylation of histone H2AX. This phosphorylated histone is often mention as γ-H2AX, and is one of the earliest DSB repair responses. The present of γ-H2AX activated many proteins in homologous recombination (HR) or non-homologous end joining (NHEJ) pathway at the damage site (*48, 49*).

Endogenous DNA double strand break (EDSBs) can occur spontaneously without any induction by exogenous factors (*50*). EDSBs are generally believed to result from a variety of events, such as stalled DNA replication through single stranded damages and mechanical stress (*51*). EDSBs often appear about 50 times per cell cycle in human cells, but most are rapidly repaired in normal cells (*50*). The majority of spontaneous DSBs are repair efficiently however inaccurate repair of EDSBs could be a cause of mutations and cancer. So, in normal cells, there should have mechanisms to avoid error-prone repair of EDSBs that could protect the genome from potentially harmful mutation or chromosomal rearrangements.

Recently, we found EDSBs in G0 (replication independent-EDSBs) (RIND-EDSBs) in many cell types without induction with radiation or DNA breaking agents (*16*). Unlike pathogenic DSBs, RIND-EDSBs may possess physiologic function to the cells. Therefore we named them as physiologic-RIND-EDSBs (phy-RIND-EDSBs). We previously noted that hypermethylated RIND-EDSBs in human cells were repaired by a more precise ATM-dependent non-homologous and joining (NHEJ), but pathogenic DSBs were commonly repaired by a fast, more error prone Ku-mediated NHEJ. The

compact structure of heterochromatin prevented H2AX phosphorylation, a conventional DSBs repair response, hypermethylated RIND-EDSBs avoiding error-prone NHEJ repair (*16*).

CHAPTER III
MATERIALS AND METHODS

Cells and culture

The tumor HeLa cell line, the human embryonic kidney HEK293, a non-tumor cell line, and the periodontal ligament PDL fibroblast were cultured in DMEM high glucose (Gibco) supplemented with 10% fetal bovine serum (FBS) (Gibco) (working culture medium) and maintained at 37 °C in a humidified atmosphere with 5% CO_2.

siRNA transfection

siRNA-Alu sequences are sense; 5'-CUUUGGGAGGCCGAGGCGGGCGGAUCA -3', antisense; 5'-AUCCGCCCGCCUCGGCCUCCCAAAGUG-3'. The day before transfection, Cells were seed at 5×10^4 cells per well of a 24-well plate in 0.5 ml of DMEM with 10% FBS. For each well in a transfection, dilute 20 µM of siRNA into 25 µl Opti-MEM medium. Mix gently. For each well in a transfection, dilute 2 µl of Lipofectamine reagent into 25 µl Opti-MEM and mix. Combine diluted DNA and diluted Lipofectamine reagent, mix gently, and incubate at room temperature for 20 min. While complexes are forming, replace the medium on the cells with 0.45 ml of DMEM growth medium. For each transfection, add the complexes onto the cells produced final concentration of siRNA-Alu was 150 nM. Incubate the cells with the complex at 37 °C in a CO_2 incubator for 2 days. After the incubation time, the cells were collected by trypsinization.

DNA preparation and quantification of DNA methylation level by COBRA (Figure 8)

Cells were harvested by trypsinization and performed DNA extraction with 10% sodium dodecyl sulfate (SDS) (Sigma), lysis buffer II (0.75M NaCl, 0.024M EDTA at pH 8) and 20 mg/ml proteinase K (USB) incubate at 50 °C over 3 nights until cell digestion. Lysed cells were extracted with phenol/chloroform and DNA was precipitated with absolute ethanol. Next, DNA sample was subjected to quantify methylation level using Combined Bisulfite Restriction Analysis (COBRA). Briefly, genomic DNA (750 ng) were

treated with sodium bisulfite using EZ DNA methylation-Gold™kit (Zymo research) base on the manufacturer's instruction. To investigate Alu methylation, the bisulfite-treated DNA was used to 35 cycle of PCR with Alu-Forward (5'-GGYGYGGTGGTTTAYG TTTGTAA-3') and Alu-Reverse (5'-CTAACTTTTTATATTTTTAATAAAAACRAAATTTCACC A-3') primers with an annealing temperature of 57 °C to generate 133 bp amplicon. The PCR amplicons were digested with two units of TaqI (Fermentas) at 65 °C overnight. The digested products were analyzed in an 8% non-denaturing polyacrylamide gel and stained with SYBR green (Lonza). The band intensity of COBRA Alu methylation observed and measured by Strom840 and ImageQuanNT Software (Amersham biosciences). Base on detection by COBRA, methylation status of the 2 CpG dinucleotide of Alu loci was into four groups including: (1) Alu loci with 2 unmethylated CpGs ($^{u}C^{u}C$); (2) Alu loci with 2 methylated CpGs ($^{m}C^{m}C$); (3) Alu loci with 5'-methylated and 3'-unmethylated CpGs ($^{m}C^{u}C$); and (4) Alu loci with 5'-unmethylated and 3'-methylated CpGs ($^{u}C^{m}C$). Four bands that differed in their Alu methylation statuses including 133 bp ($^{u}C^{u}C$), 90 ($^{m}C^{u}C$), 75 ($^{u}C^{m}C$), 58, and 32 ($^{m}C^{m}C$), were quantified (Figure 8). The intensity of each band was divided by its paired length as followed: 133 bp/133 (A), 58 bp/58 (B), 75 bp/73 (C), 90 bp/90 (D) and 43 bp/41 (E). The Alu methylation level (overall or total) was calculated as the percent of the methylated bands (^{m}C) intensity divided by the sum of the ^{m}C and unmethylated bands (^{u}C) intensities, [(E+B)/(E+B+2A+C+D)]×100. Similarly, to evaluate LINE-1 methylation, the bisulfite-treated DNA was amplified with LINE-1-Forward (5'-CCGTAAGGGGTTAGGGAGTTTTT-3') and LINE-1- Reverse (5'-RTAAAACCCTCCRAACCAAATATAAA-3') primers with an annealing temperature of 50 °C to generate 92 bp PCR amplicon. The PCR products were digested with two units of TaqI and TasI (Fermentas) at 65 °C overnight. The digested products were analyzed as describe above. Four bands that differed in their LINE-1 methylation statuses comprise of 92 bp ($^{m}C^{u}C$), 60 bp ($^{u}C^{u}C$), 50 ($^{m}C^{m}C$) and 18 ($^{u}C^{m}C$) bp, were quantified. The intensity of each band was divided by its paired length as followed: 92 bp/92 (A), 60/56 (B), 50/50 (C), 42/40 (D), 32/28 (E), 18/14 or [(D+E)-(B+C)]/2 (F). The LINE-1 methylation level (overall or total) was calculated as the

percent of the methylated bands (^{m}C) intensity divided by the sum of the ^{m}C and unmethylated bands (^{u}C) intensities, [(A+2C+F) /(2A+2B+2C+2F)] ×100.

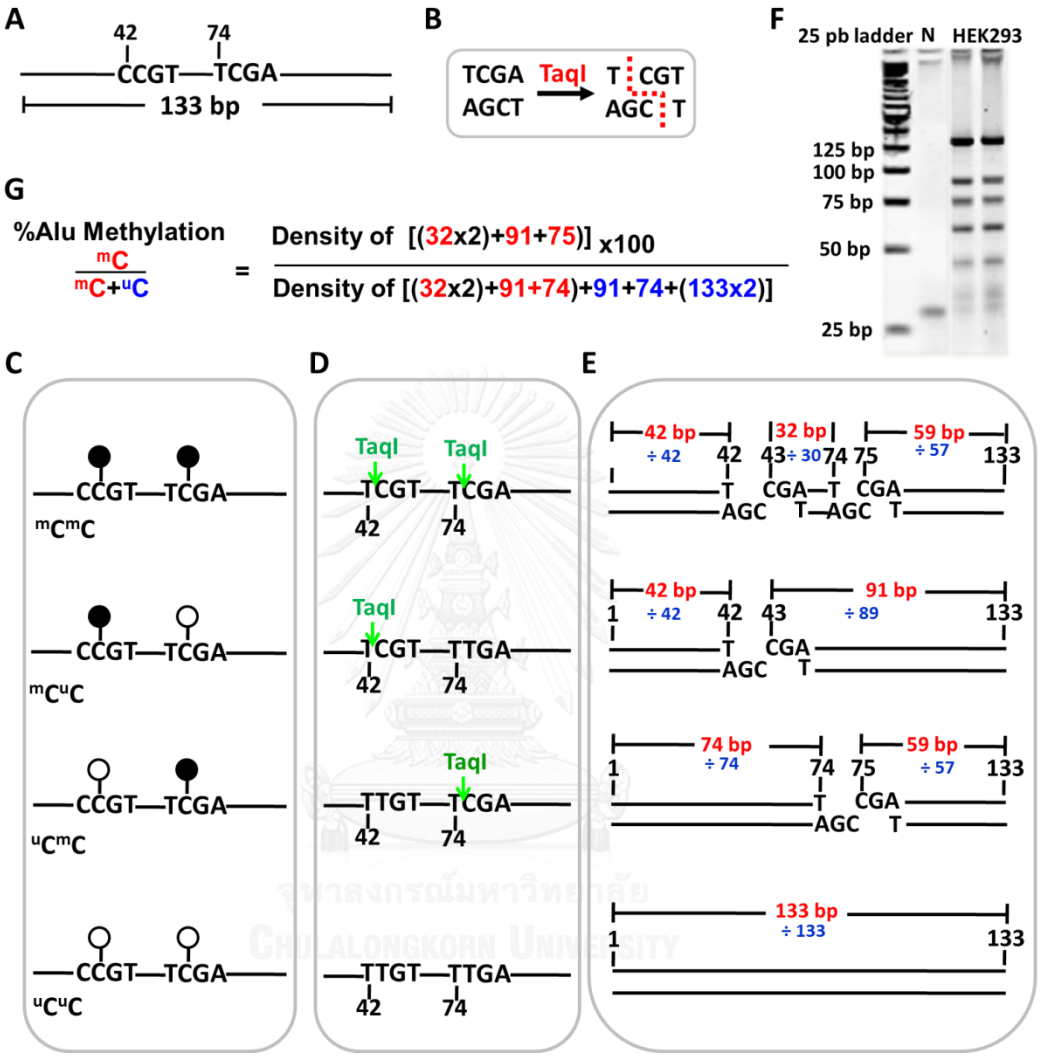

Figure 8 The methylation patterns of Alu detected by COBRA-Alu. **(A)** COBRA of The Alu sequence contains two CpG dinucleotide loci, and the PCR amplicon size of Alu is 133 base pairs. **(B)** Restriction enzyme TaqI (TaqI) has the recognition sequence of is 5'TCGA or 3'AGCT and makes the cohesive end cut 5'---T CGA---3' or 3'---AGC T---5'. **(C)** There are four possible methylation patterns of the Alu sequence. The black and white circles represent methylated and unmethylated cytosine, respectively. COBRA-Alu separated the detecting region into four products: mCmC, uCuC, mCuC and uCmC. **(D)** After the bisulfite treatment and PCR amplification the unmethylated cytosine residues

are converted to uracil and thymine, respectively, but the methylated cytosine residues are unaltered. This leads to retention or loss of CpG containing restriction enzyme sites. **(E)** The PCR products are digested with TaqI. **(F)** Representative gel image for COBRA-Alu assay. Lane 1: 25 bp markers, Lane 2: negative control (N), Lanes 3-4: DNAs from HEK293 cells. **(G)** The equation used to calculate percent of Alu methylation level.

Alu methylation evaluation by Ion Torrent sequencing and sequence analysis (Figure. 9)

DNA from siRNA-Alu transfected cells was extracted, bisulfite treated and amplification as described above. The PCR products were sent to sequencing by Ion Torrent sequencer (Ion Torrent™ Personal Genome Machine® (PGM), Life Technologies, USA).

For each sample, we aligned each read against siRNA sequence, then calculated a percent identity (PID) from an alignment and examined if an alignment contained any insertion and deletion (INDEL). Next, we performed a second alignment on each read against an insert sequence (ALU sequence). There were four CpG positions in an insert sequence; therefore, we determined whether C or T was present at each position from the result of the second alignment. Since si-RNA sequence's length was 27, PID occurred at only certain percentage (i.e. 100%, 96%, 93%, 89%, and so on). We sum the number of C and the number of T at each position from reads that had the same length, and had PID greater than and less than or equal to a certain PID value (all possible values were used). The summing step was done separately between reads whose alignments contained INDEL and without INDEL. Next, we calculated the percentage of C (%C) at each position and each length. We performed Student's t-test between samples with and without added si-RNA based on %C at each position and each read length. The p-values were used to plot graphs.

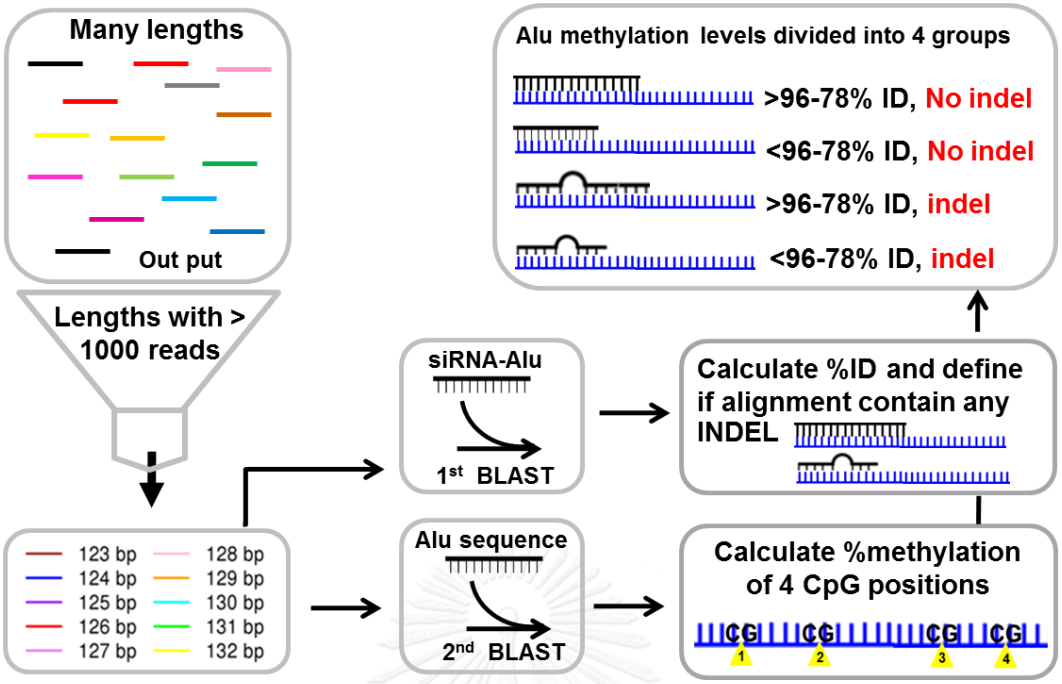

Figure 9 Work flow of Alu methylation Ion torrent data and analysis. First, for each sample, lengths of reads greater than 1000 reads were selected. There is product size from 123-132 base pair (color shading) and aligned each read against siRNA sequence, then calculated a percent identity (ID) from an alignment and defined if an alignment contained any insertion and deletion (INDEL). Next, each read was performed a second alignment on against an insert sequence (ALU sequence), then calculated a percent of four CpG positions in an insert sequence. Therefore, Alu methylation level, which determined by Ion Torrent sequencing, was divided into four groups base on %ID (96-68%) and with or without insertion/deletion (INDEL).

Proliferation assay

Cell proliferation assay was performed briefly, 2,000 cells (20,000 cell/ml) were seeded in 96-well plate containers in 100 µl media. Cell proliferation was assessed using the MTT reagent (MTT assay) (sigma) for 4 days starting 24 hours after cell seeding. Moreover, total cell number was counted after seeding siRNA-Alu transfected cells over 4 days (cell count assay) (*52*).

Determination of population doubling of cells

Population doublings was determined using the following equation: D = ((B-A(2^n)/(A(2^{n+1})-A(2^n))). Where A equals no. of cells plated, B equals no. of cells counted after growth period, C equals old population doubling, D equals new population doubling and *n* equals the largest number that satisfies the equation A(2^n) ≥ B (*53*).

Cell cytotoxicity assay

Cells were seeded at 4,000 cells in 100 µl (40,000 cells/ml) to 96-well plate. Twenty-four hours later, cells were treated with medium containing an increasing concentration of methyl methanesulphonate (MMS) (Sigma) (0-2 mM) and hydrogen peroxide (H_2O_2) (Sigma) (0-150 µM) for one and 24 hours, respectively, in a CO_2 incubator. Then the media containing MMS was replaced with normal working media. Cell growth was measured with MTT assay 48 hours after treatment (*54, 55*).

Determination of 8-OHdG and AB site

8-hydroxy-2'-deoxyguanosine (8-OHdG) and AP site levels in both peripheral blood of healthy individuals and cell lines were analyzed using OxiSelect™ Oxidative DNA Damage ELISA Kit (8-OHG Quantitation) and OxiSelect™ Oxidative DNA Damage ELISA Kit (AP site Quantitation) (Cell BioLabs) according to the manufacturers' protocol.

Statistical analysis

For comparisons between two independent groups, the independent sample t-test was used for normally distributed data, and the Mann-Whitney test was used for skewed data. Pearson's correlation test was used to assess the correlation between continuous variables. SPSS version 17.0 (SSPS Inc., Chicago, IL) and GraphPad Prism 5 (GraphPad software Inc., California USA) were used for all calculations. A P value, 0.05 was considered statistically significant.

Yeast strains, media and growth conditions

Yeast strains used in this study were BY4741, *ypr052cΔ* (*nhp6aΔ*), JKM115 (*MATΔ ΔhohmlΔ::ADE1 hmrΔ::ADE1 lys5 leu2 ura3 trp1*), JKM179 cells (*MATΔ ΔhohmlΔ::ADE1 hmr: Δ:ADE1 lys5 leu2 ura3 trp1ade3::GALHO*) and YAA25 (+HO, *mec1Δ sml1Δ)* from the same sources as previously described (*19, 56*). For chronological aging experiments, yeast cells were grown in YP + 2% glucose at 30°C 250 rpm overnight and then switched to YP + 2% raffinose for 2 days before being washed and resuspended in sterile deionized water. Cells in the G0 phase were determined by their morphology under a microscope. All cells of all yeast strains consisting of G0 phase cells (100% unbudded stationary-phase cells). To inhibit the ATM/ATR-dependent DNA repair pathways, yeast cells were treated with 10 mM caffeine (Sigma, USA) 24 hours (*57*).

HO induction and caffeine treatment

For HO induction and caffeine treatment, JKM115, JKM179 and YAA25 were used (*58*). Therefore, this galactose-induced DSB cannot be repaired by homologous recombination. Expression of the HO endonuclease was induced by the addition of galactose to the media for 3 hours. After induction, cells were placed in media containing 2% glucose to repress HO expression and washed with sterile deionized water. Approximately 1×10^8 cells/ml were resuspended in sterile deionized water (0 hr) and maintained at 30°C in a rotary shaker at 250 rpm. After HO induction, cell viability was measured by plating an aliquot of the culture on a YPD plate and counting the number of visible colony forming units (CFUs).

Genome wide EDSB ligation mediated PCR and high throughput sequencing (Figure 10)

High-Molecular weight DNA was performed as previously described (*19*). To prepare HMW DNA, yeast cells were treated with 1 mg/ml lyticase (70 U/mg) (Sigma) for 2 hours and embedded in 1% low melting point agarose at a concentration of 2×10^8 cells per plug. Embedded cells were digested in 400 µl of digestion buffer (1 mg/ml

proteinase K, 50 mM Tris, ph 8.0, 20 mM EDTA, 1% sodium lauryl sarcosine) at 37 °C overnight. Theplugswrerinsed6 times in TE buffer for 40 minutes. EDSBs with cohesive ends were polished by incubating with T4 polymerase (New England Biolabs) and dNTPs for 1 hour. The enzyme was inactivated by adding EDTA at a final concentration of 20 mM, for 5 minutes, and rinsed 6 times in TE buffer for 40 minutes. The modified LMPCR linkers were prepared from oligonucleotides: 5'-AGGTAACGAGTCAGACCACC GATCGCTCGGAAGCTTACCTC GTGGACGT-3' and 5'-ACGTC CACGAG-3'. The linkers (50 pmol) were ligated to the polished EDSB ends in the HMW DNA preparations using T4 ligase (New England Biolabs) at 25 °C overnight. Linker-ligated DNA was then extracted from the agarose plus using a QIAquick gel extraction kit (Qiagen).

Library preparation and EDSB sequencing were performed as previously described (Pongpanich et al., 2014). Briefly, the HMW DNA was subjected to 60 cycles of PCR with two primers, First-L-F (5'-AGGTAACGAGTCAGACCACCGA-3') and Second-L-R (5-GGTACCGGT AGGGCCTACGGGT-3' (Sigma) using an annealing temperature of 65°C. The PCR product was purified with a QIAquick PCR Purification Kit (Qiagen, Switzerland) and sequenced on an Ion Torrent sequencer (Ion Torrent™ Personal Genome Machine® (PGM), Life Technologies, USA). The raw sequencing data have been deposited in the Sequence Read Archive (SRA) under the accession number SRP073848, SRP074023 and DDBJ Sequence Read Archive (DRA) under the accession number DRA002436.

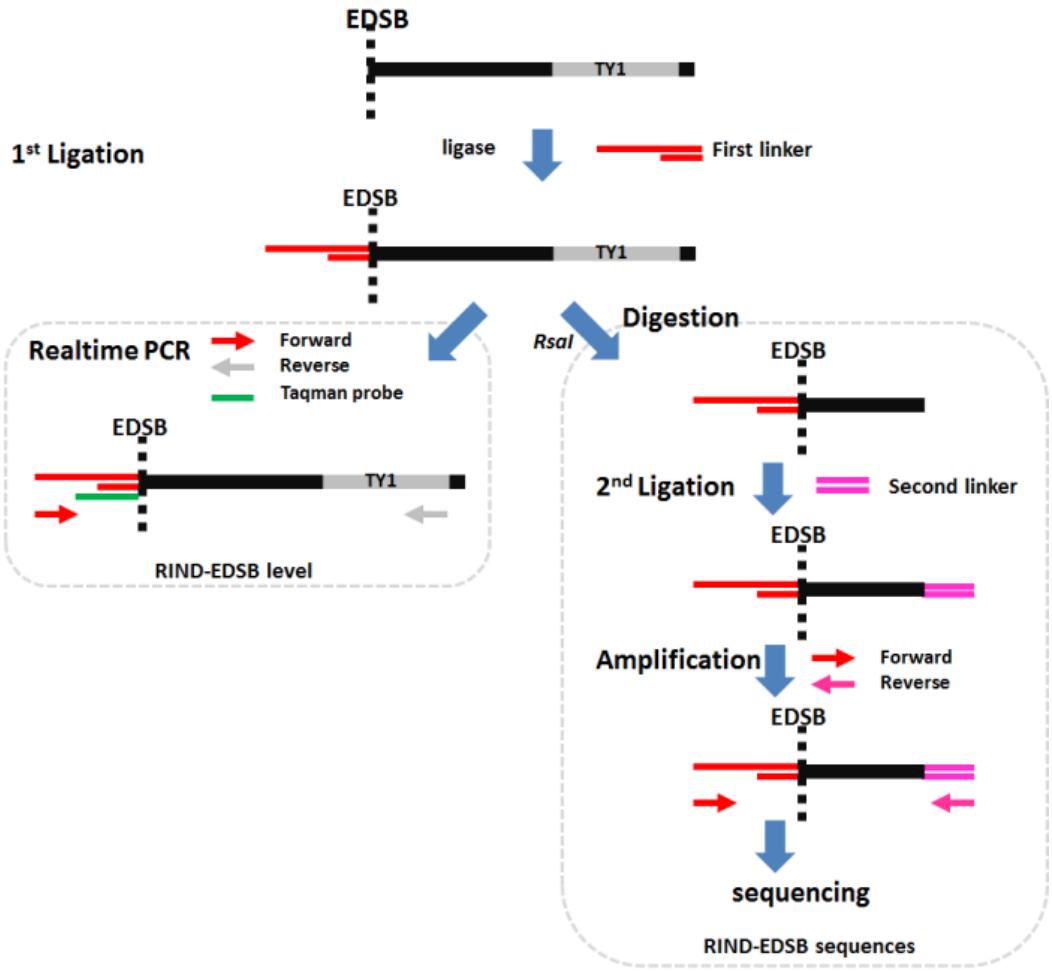

Figure 10 Schematic representation of RIND-EDSB-detection using real-time PCR and RIND-EDSB pattern sequences using Ion Torrent sequencer. The black and vertical dashed lines represent genomic DNA and EDSB end, respectively. The red parallel line is the first linker sequence. The grey line represents TY1 elements which are long terminal repeat (LTR) retrotransposons. The red and grey arrows represent the forward and reverse primers, respectively. The green line is TaqMan probe. In the first step, the first linker is ligated to one of the EDSB ends. Next, the first ligated DNA is used as subject for measuring RIND-EDSB level using TaqMan real-time PCR assay. To study the RIND-EDSB sequences, the first ligated DNA is digested with a restriction enzyme, RsaI, which does not cut within linkers. Next, the second linker is ligated to the digested DNA. Finally, EDSBs were amplified with primers that bind to the first and second linker and sequenced on an Ion Torrent sequencer.

Linker-mediated Ion torrent data processing and analysis (Figure 11)

Reads from the Ion torrent sequencing data contained linkers at both ends, which we removed using the trimming pipeline described previously (*19*). Next, the trimmed reads were aligned using Nucleotide-Nucleotide BLAST 2.3.0 + (35). For JKM179, the caffeine treatment, HO induction, and combined caffeine treatment with HO induction reads were mapped against reads from a whole genome sequencing (WGS) dataset for JKM179. Each mapped read was either mapped from the first base or not from the first base. We called reads that were not mapped from the first base as reads with Modified ends with Insertion at the Breaks (MIB). For reads without MIB sequence, we obtained four bases preceding each of the aligned positions, which corresponded to a break position. If a read mapped to multiple WGS reads (multi-mapped reads), we retained only reads that had all the same four preceding bases. The remaining unmapped reads were then aligned against the BY4741 genome using BLAST 2.3.0+. The preceding four bases were also obtained for each alignment. We retained multi-mapped reads if the preceding four bases were all the same (same condition as in WGS alignment). For *nhp6aΔ*, *nhp6aΔ* treated with caffeine, wild-type day 0, and wild-type day 50, reads were mapped against BY4741, the preceding four bases were obtained, and the same criteria were used in retaining reads as previously stated. Wild-type day 0 was the sample published previously (Pongpanich et al., 2014). Next, we counted the number of reads with MIB sequences.

Afterward, for each sample, we obtained raw counts by counting how many reads had the preceding four bases (4-mer) as AAAA, AAAC, and so on; there were 256 possible 4-mer combinations (AAAA, AAAC, …, TTTT). We calculated actual counts by dividing raw counts by total reads and multiplying by the levels of the measured EDSBs per Mb. We also counted the occurrence of each four-base combination in the WGS data and in the BY4741 reference genome. Then, we constructed a 2×2 contingency table for each 4-mer combination in the JKM179 sample, where the rows were JKM179 sample vs. WGS data and the columns were one of the 4-mer sequence raw counts vs.

the rest of the 4-mer sequences. We also constructed a similar contingency table for wild-type day 0, but the rows were wild-type day 0 vs. the BY4741 reference genome. Odds ratios (OR) were then computed from these contingency tables. Next, we acquired 4-mer combinations with OR>1 in the JKM179 sample (the 179 first group) and 4-mer combinations with OR<=1 in the JKM179 sample (the 179 second group). For the JKM179, caffeine treatment, HO induction, and combined caffeine treatment with HO induction sequences, we summed all the actual counts of the 4-mer combinations under the 179 first group and then under the 179 second group. Similarly, we acquired 4-mer combinations with OR>1 in the wild-type day 0 sample (the wild-type day 0 first group) and 4-mer combinations with OR<=1 in the wild-type day 0 sample (the wild-type day 0 second group). For the *nhp6aΔ*, *nhp6aΔ* treated with caffeine, wild-type day 0, and wild-type day 50 sequences, we summed all the actual counts of 4-mer combinations under the wild-type day 0 first group and then under the wild-type day 0 second group.

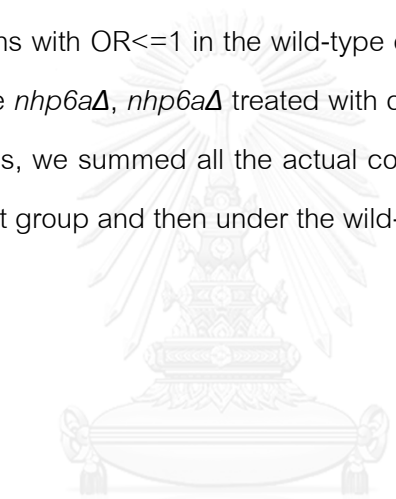

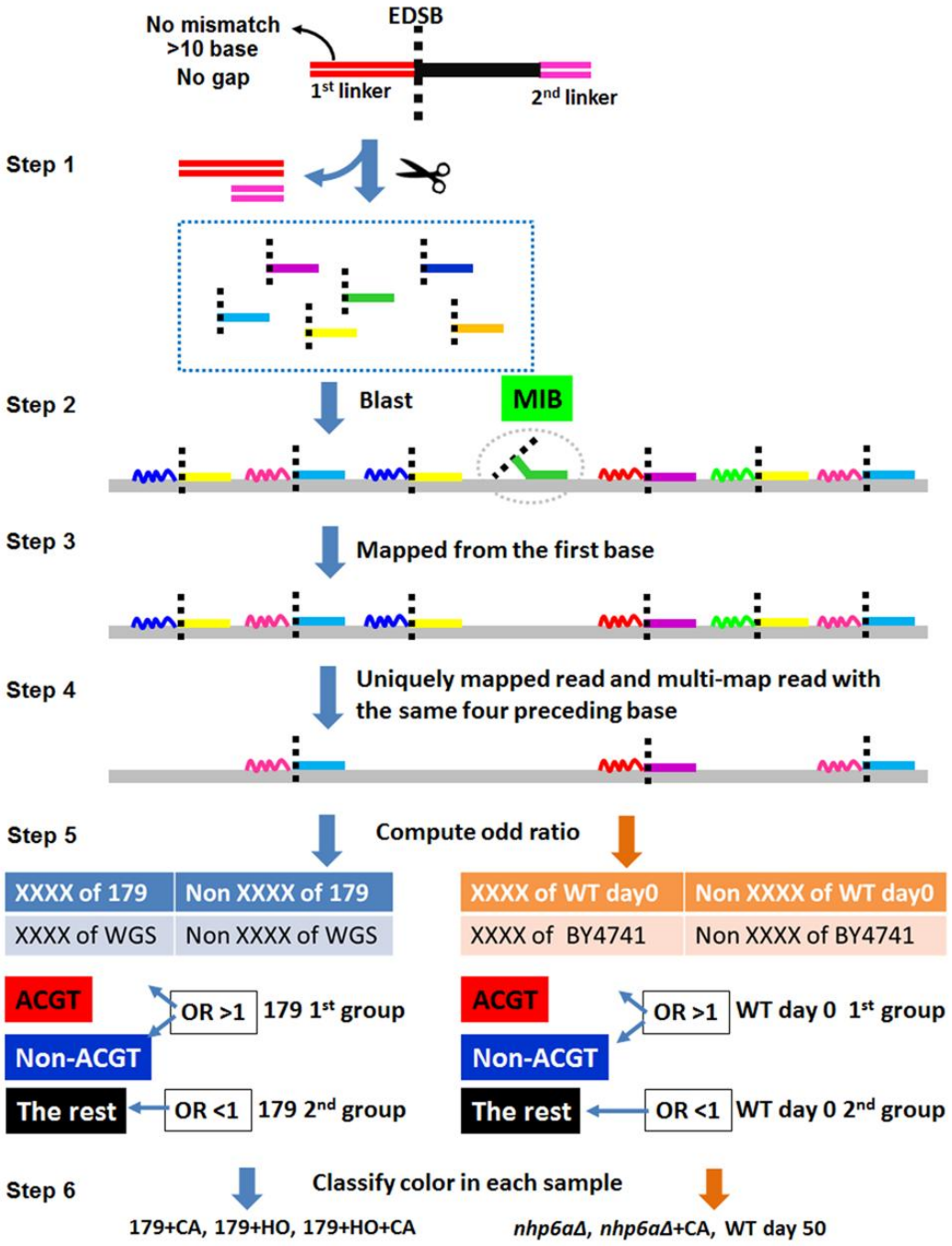

Figure 11 Work flow of Linker-mediated Ion torrent data processing and analysis. There are six steps in the workflow1; (1) Reads of length greater than 10 bases and contain no mismatch and no gaps in the First linker were retained after trimming linkers. (2) BLAST the trimmed reads of JKM179, the caffeine treatment, HO induction, and combined caffeine treatment with HO induction to reads from a whole genome sequencing (WGS) dataset of JKM179 and BLAST the trimmed reads of *nhp6aΔ*, *nhp6aΔ* treated with

caffeine, wild-type day 0, and wild-type day 50, against BY4741. (3) Retain reads from BLAST results that are aligned from the first base (4) Obtain four bases preceding each of the aligned positions, which corresponded to a break position. If a read mapped to multiple WGS reads (multi-mapped reads), we retained only reads that had all the same four preceding bases. (5) Compute odds ratio for each 4-mer of JKM179 by performing a 2×2 contingency table based on WGS data and compute odds ratio for each 4-mer of wild type day 0 by performing a 2×2 contingency table based on BY4741. (6) Classify colors in each sample of the caffeine treatment, HO induction, and combined caffeine treatment with HO based on odd ratio of JKM179 and classify colors in each sample of *nhp6aΔ*, *nhp6aΔ* treated with caffeine, and wild-type day 50 base on odds ratio of wild type day 0.

CHAPTER IV
RESULTS

Alu methylation and DNA damage

DNA damage, an alteration in the chemical structure of DNA, is a precursor to mutation, cellular senescence and cell death. The seven most common steady state endogenous DNA damages in mammalian cells are abasic sites (AP site), N7-(2-hydroxethyl)guanine (7HEG), 8-hydroxyguanine (8-OHdG), 7-(2-oxoethyl)guanine, formaldehyde adducts, acrolein-deoxyguanine, and malondialdehyde-deoxyguanine, respectively (*7*). Here, we chose to determine AP sites and 8-OHdG because they are prevalence and practical.

First, the determinations of the 8-OHdG and plasma Alu methylation level were performed in healthy people. The healthy people (n = 28) were between 44 and 68 years of age (59.96 ± 5.73 years) and consisted of 5 (82.14%) males and 23 (14.75%) females. In the healthy people, we found a strong, negative linear correlation between the 8-OHdG and Alu methylation in circulating blood cells (r = -0.5871, P = 0.0013) (Figure 12A). Similarly, we also detected the negative linear correlation between Alu methylation in circulating blood cells and AP sites (r= -0.5058, P = 0.0071) (Figure 12B).

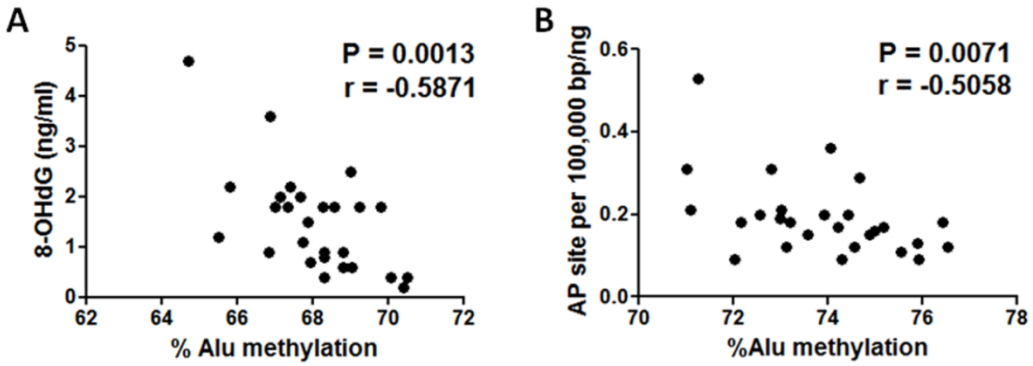

Figure 12 A univariate correlation analysis between the levels of DNA damages and Alu methylation in peripheral blood cells of the healthy people. **(A)** The 8-OHdG was linearly negative correlated with the Alu methylation levels. **(B)** AP site was linearly negative correlated with Alu methylation levels. r: Pearson's correlation coefficient. The displayed P values are from the Pearson's correlation test.

Increase in Alu methylation level was observed in cells with siRNA-Alu transection

The result of correlation analysis suggested that loss of DNA methylation in Alu elements accompanies with more endogenous DNA damages which represent the imbalance between formation and repair or genomic instability. This finding lets us address the question that if increasing Alu methylation would improve genomic instability or decrease DNA damage. According to present knowledge, there is RNA directed DNA methylation (RdDM) mechanism, so we chose this mechanism as the treatment to modify Alu methylation levels.

Then, to test if Alu-siRNA can promote methylation at Alu loci, we transfected an increasing concentrations of siRNA-Alu to HeLa, a cervical cancer cell line, and HEK-293, a human embryonic cervical cancer cell line, significantly increased in level of Alu methylation was observed in both HeLa (Figure 13A) and HEK293 cells (Figure 13B). Moreover, significantly increasing Alu methylation also found even though methylation level was calculated separately in each position (Figure 14).

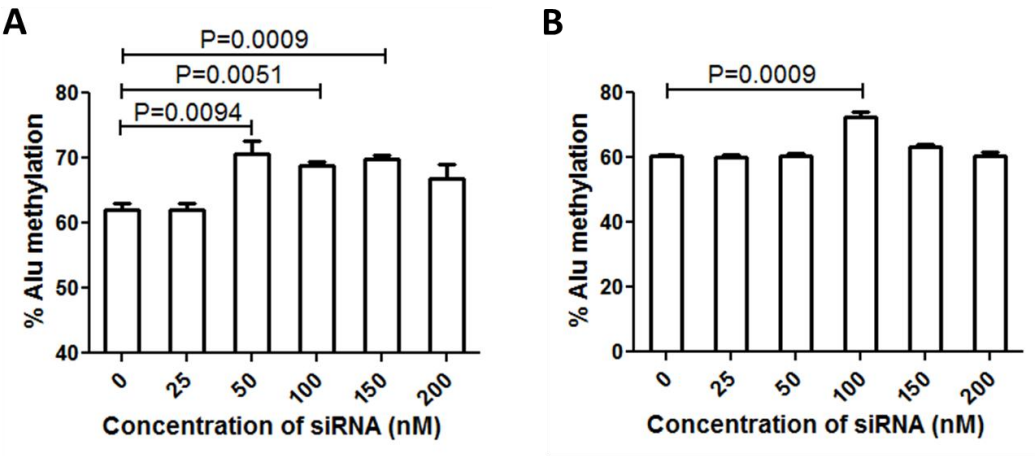

Figure 13 Percentage of Alu methylation level in cells transfected with siRNA-Alu at various increasing concentrations (0-200 nM). **(A)** The percentage of total (overall) Alu methylation levels in non- tumor human embryonic kidney cells (HEK293) significantly increased at the concentration of 50, 100 and 150 nm. **(B)** The percentage of total (overall) Alu methylation levels in cervical cancer cell (HeLa) significantly increased at the only one concentration of 100 nM.

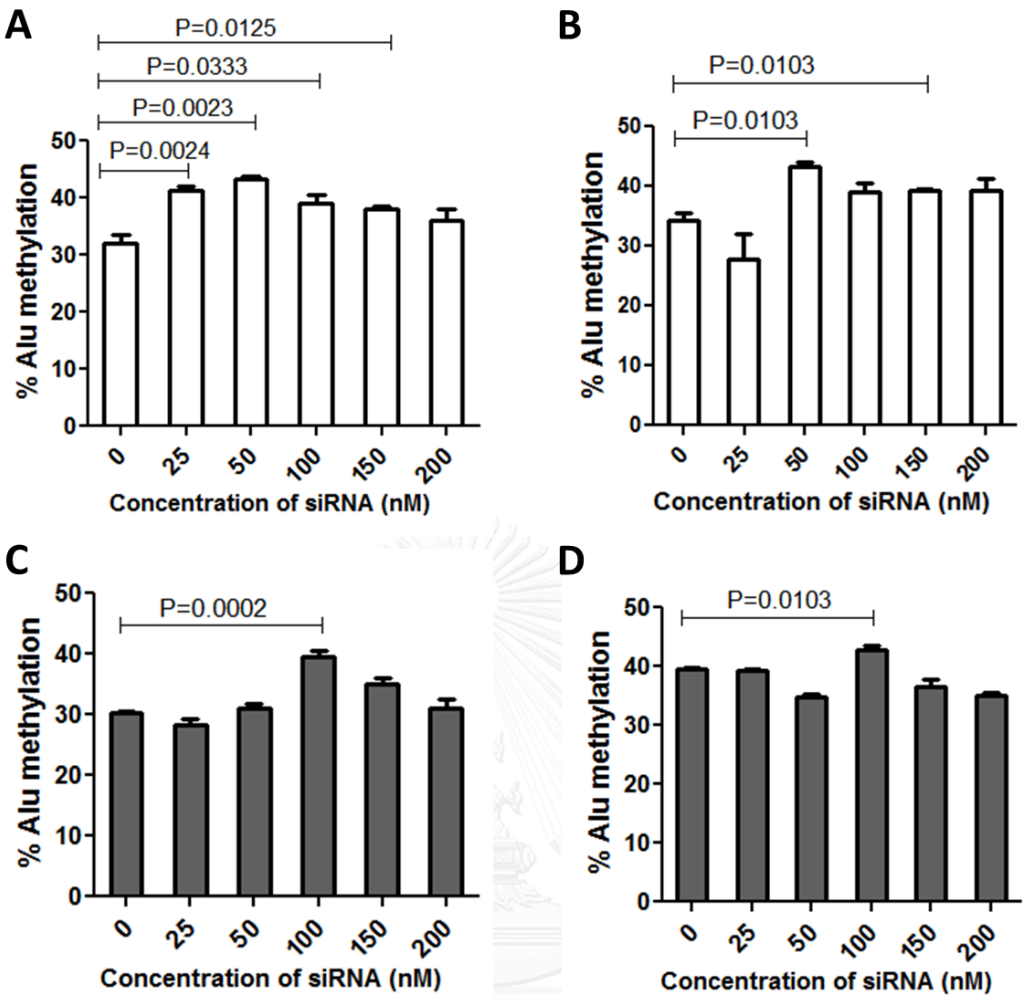

Figure 14 The percentage of Alu methylation levels of each position in HEK293 (white bar) and HeLa (grey bar) cells. **(A and C)** The percentage of Alu methylation levels of the first CpG position (siRNA-Alu binding site). **(B and D)** The percentage of Alu methylation levels of the second CpG position.

Moreover, the de novo methylation was sequence specific. There was no change in LINE-1 methylation (Figure 15).

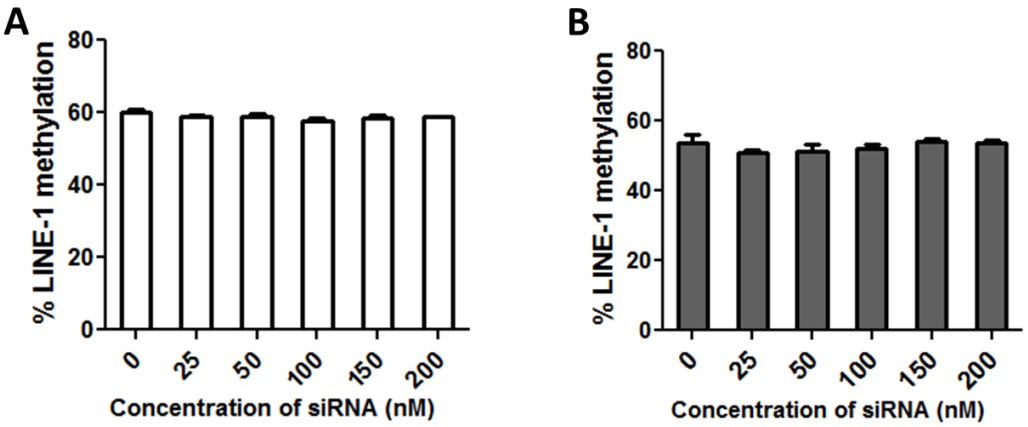

Figure 15 The percentage of LINE1 methylation levels of cells with siRNA-Alu transfection. **(A)** The percentage of LINE1 methylation levels in transfected HEK293 cells. **(B)** The percentage of LINE1 methylation levels in transfected HeLa cells.

Interestingly, the methylation was sustainable because HEK293 also resulted in an increase in Alu methylation level after continue cell culture at 7 days (Figure 16).

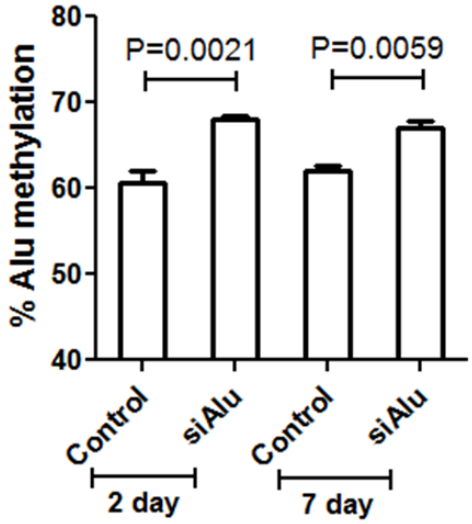

Figure 16 The percentage of Alu methylation at day 2 and day 7 in HEK293 cells after transfected with siRNA-Alu (150 nM). The Alu methylation level of HEK293 cells with siRNA-Alu transfection was significantly increased at both day 2 and day 7 after transfection.

To compare between siRNA binded Alu sequences and Alu methylation of each allele, we performed ion torrent sequencing and compared DNA methylation levels between siRNA-Alu transfected to HEK-293 and control. Ion torrent sequences yielded Alu amplicon varied in lengths. We plotted graphs on $-\log_{10}$(p-values) of read length from 123 to 132, possessed high yield sizes, for all four CpG nucleotide positions (CpG1-4) We grouped $-\log_{10}$(p-values) by siRNA binding sites having insertion or deletion (indel) and percent identity (%ID) value. Figure 2D showed $-\log_{10}$(p-values) for each length in separate columns and separate graphs for each %ID. 100% ID corresponds to perfect match between si-RNA sequence and Alu sequence. Figure 2D illustrated that having indel and no indel in an alignment yielded different results. P-values were significant at significance threshold of 0.005 at certain read length (mostly at 123-126) and certain position (mostly at the first and fourth position) when %ID was high (but need not be 100%), and %ID can be lower if indel was absent in the alignment (Figure 17).

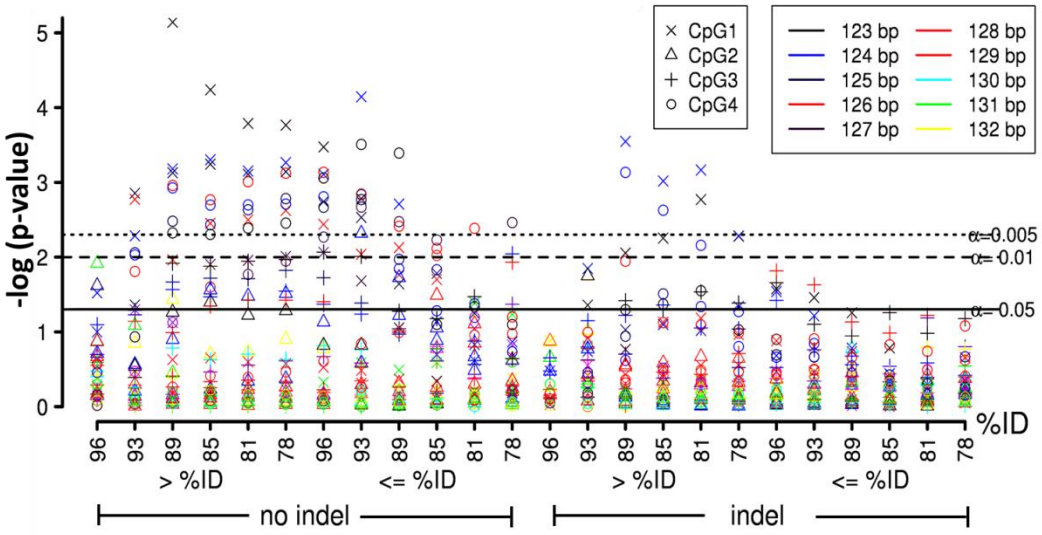

Figure 17 Alu methylation of each allele using high-throughput sequencing. –log10(p-values) from Student's t-test between siRNA-Alu transfected HEK-293 and control of Alu methylation pattern of four CpG locations with PCR product size ranging from 123-132 base pairs (color shading) categorized by % identity to siRNA sequence (%ID) (78-96%) and the presence and absence of insertion/deletion (indel). Solid, dashed, and square dotted lines represent significant levels at 0.05, 0.01, and 0.005, respectively.

Above resulted from the experiment in immortal cell lines. We will soon apply these finding as underlying mechanism to increase Alu methylation of aging cells because Alu is heavily methylated but theses methylation is reduced in aging cells. Therefore, PDL (periodontal ligament) fibroblast, which is human diploid cells have a limited number of cell dividing, were used to transfect with siRNA-Alu. The level of Alu methylation was significantly increased in siRNA-Alu transfected cells (Figure 18).

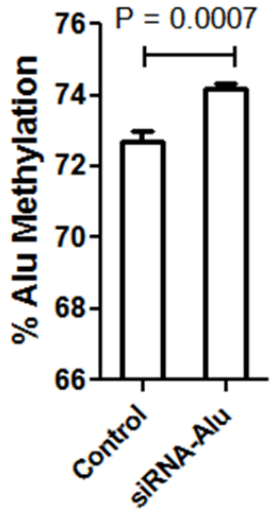

Figure 18 The percentage of Alu methylation level in periodontal ligament (PDL) fibroblast (passage 10) transfected with siRNA-Alu (150 nM). The level of Alu methylation was significantly increased in cells with siRNA-Alu transfection.

Hypermethylated Alu cells proliferated faster than control cells

Then, we investigate the phenotypic change of increasing of Alu methylation. First by assessment of cell proliferation, using the MTT assay, we observed a significantly increased rate of proliferation in HEK293 cells with siRNA-Alu transfection (Figure 19A). We also confirmed this result by counting absolute cell numbers after seeding siRNA-Alu transfected HEK293 cells over 4 days (Figure 19B), with again show a similarly increased rate of cell proliferation in siRNA-Alu transfection. To further support this result, we performed MTT assay in PDL fibroblast cells with siRNA-Alu transfection and increasing Alu methylation was proved, the rate of proliferation of hypermethylated fibroblast cells was significantly faster than control cells (Figure 19C). Next, to increase the confident of that proliferation results, we counted cell numbers of PDL cells after transfection at the passage 13 and 14 and calculated to population doubling (PD) value which is more accuracy. Likewise, we found that cells with siRNA-Alu generated significant higher PD value than control cells in both passage 13 and 14

(Figure 19D). Taken together, we proposed that Alu methylation altered cellular phenotypes. Hypermethylated Alu cells proliferated faster than control cells.

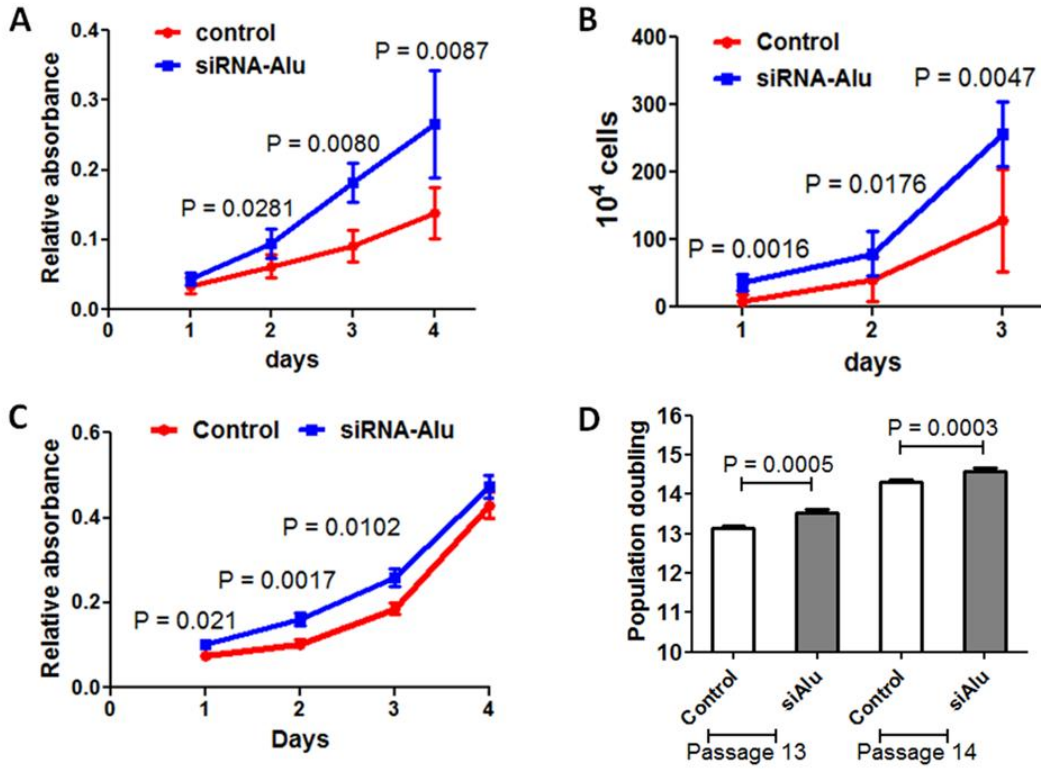

Figure 19 Proliferation in siRNA-Alu transfected cells. After transfection, cells were incubated for 48 hours. Then the transfected cells were seeded into 96-well plate for proliferation evaluation. (A and B) Cell proliferation in HEK293 was assessed by MTT over 4 days after siRNA-Alu transfection **(A)** and absolute cell number was counted after seeding siRNA-Alu transfected cells over 3 days **(B)**. (C and D) Cell proliferation in PDL cells was assessed by MTT over 4 days after siRNA-Alu transfection **(C)** and population doublings of siRNA-Alu transfected cells was calculated at passage 13 and 14 **(D)**.

Alu methylation is important for resistance to DNA damage

According to the results of proliferation, we addressed the question that why hypermethylated Alu cells proliferated faster than control cells. First, we think about what matter can effect progression of cell cycle. Base on principle of cell division, there are cell cycle control or checkpoint. Whenever damages were detected, cells can arrest

until defects are repaired. We hypothesize that Alu hypermethylation would reduce DNA damages therefore cells could push normal progression through cell cycle.

To prove this possibility, cells of control and siRNA-Alu transfection with significant increasing Alu methylation level were exposed to the increasing concentration of DNA damage agents including MMS and H_20_2. Exposure of HEK293 and PDL cells to MMS showed that %cell survival of hypermethylated Alu cells was significant higher than control cells in the concentration of 1.0 and 2.0 mM (Figure 20A and 20B). Likewise, Exposure of these cells to H_20_2 demonstrated significant higher of %cell survival in hypermethylated Alu cells than control cells (Figure 20C and 20D). Our results suggested that MMS and H_2O_2 sensitivity of HEK293 and PDL cells depend on the Alu methylation levels or gave possible that increasing Alu methylation is important for resistance to DNA damage.

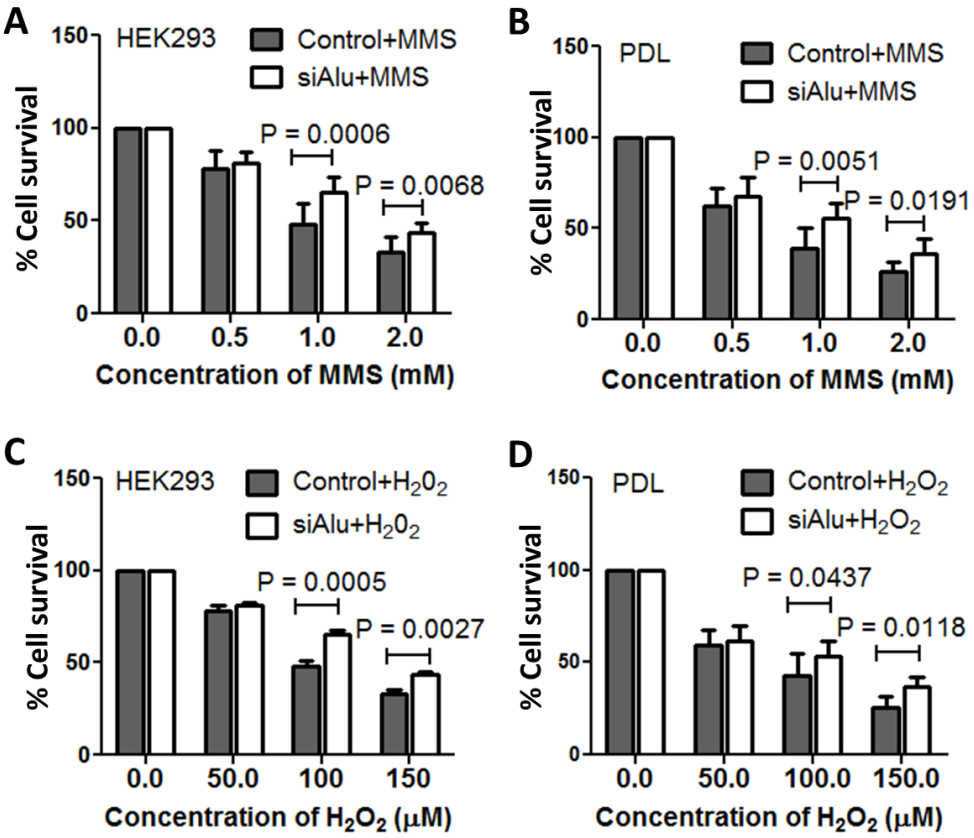

Figure 20 Hypermethylated Alu cells had a decreased sensitivity to DNA damage agent. After a significant increase in Alu methylation level confirmation, control and siRNA-Alu transfected cells were exposed to the increasing concentration of MMS for 1 hour and H_2O_2 for 24 hours. Then growth was assessed by MTT after 48 hours. Error bars indicates ± SD. (A and B) MMS sensitivity of HEK293 **(A)** and PDL **(B)**. (C and D) H_20_2 sensitivity of HEK293 **(C)** and PDL **(D)**.

In addition, genomic instability can be defined as the imbalance between formation and repair leading to DNA damage accumulation. Many previous studies proposed that endogenous DNA damage as a source of genomic instability. To further support the hypothesis that Alu hypermethylation would reduce DNA damages therefore cells could push normal progression through cell cycle therefore we investigated the level of endogenous DNA damage in control and siRNA-Alu transfected cells. The most vulnerable site for oxidative damage to DNA is on guanosine, specifically at the position C-8 leading to the production of 8-OHdG. 8-OHdG levels were measure using

OxiSelect™ Oxidative DNA Damage ELISA Kit. Interestingly, we found significant lower of 8-OHdG level in Alu hypermethylated cells than control cells (Figure 21).

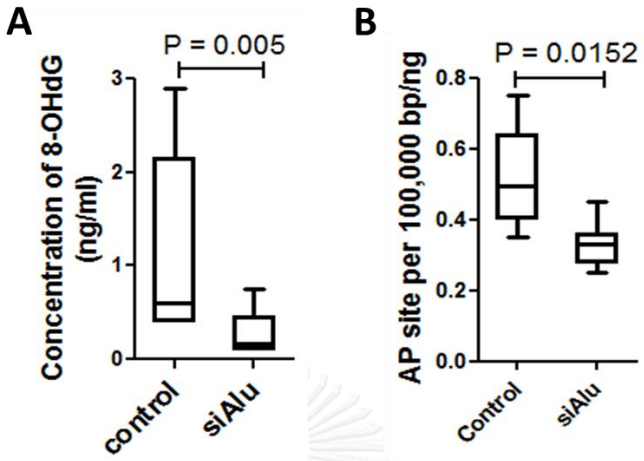

Figure 21 A comparison of 8-OHdG and AP site level in HEK293 cells between control and siRNA-Alu transfected cells. The level of 8-OHdG (ng/ml) **(A)** and AP site (per 100,000 bp/ng DN) **(B)** was significantly increased in cells with siRNA-Alu transfection.

RIND-EDSB sequences in chronological aging yeast

As we mentioned above, another important molecular mechanism underlying genomic instability is DNA double strand breaks (DSBs) and DSB repair. In our previous work, we discovered that there are two distinct types of Endogenous DNA Double strand break (EDSBs) in non-replicative cells. The first type is pathologic DNA lesions, pathologic-RIND-EDSBs. Whereas, the other, namely physiologic-RIND-EDSBs (phy-RIND-EDSBs), we hypothesized that RIND-EDSBs possess physiologic function in maintaining genomic stability.

We described RIND-EDSB sequences based on 4 nucleotides located upstream to the break. In control yeast, the 4 bp sequences were not random. As previously reported (*19*), ACGT (ACGT breaks) was the most common. The 4 bp that was found more frequently (odds ratio > 1) was named Non-ACGT breaks. Here, we named breaks containing 4 bp that were unlikely to be found (odds ratio <1) as the rest. Nevertheless,

there were some RIND-EDSBs that 5' end sequence downstream to the break did not match with genomic sequence. We called these breaks MIB. Here, we grouped all MIB together regardless of the 4 bp upstream sequences (Figure 22B). Therefore, here, we classified patterns of RIND-EDSB sequences into four groups including MIB, ACGT breaks, Non-ACGT breaks and The rest. The main objective of this study was to evaluate the alterations of RIND-EDSB sequences and quantities due to the aging process in non-dividing yeast.

At 50 days, the viability of wide type yeast (BY4741) significantly reduced. Likewise, we also found that the overall number of RIND-EDSBs was reduced (Dr. Jirapan, unpublished data). We questioned how viability and RIND-EDSBs changed during chronological aging. We found that at 50 day while the overall number of RIND-EDSBs was reduced, the percentage of ACGT breaks and Non-ACGT breaks were reduced (Figure 22A, 22B, and 22C). Therefore, chronological aging yeast had lower of ACGT and Non-ACGT breaks.

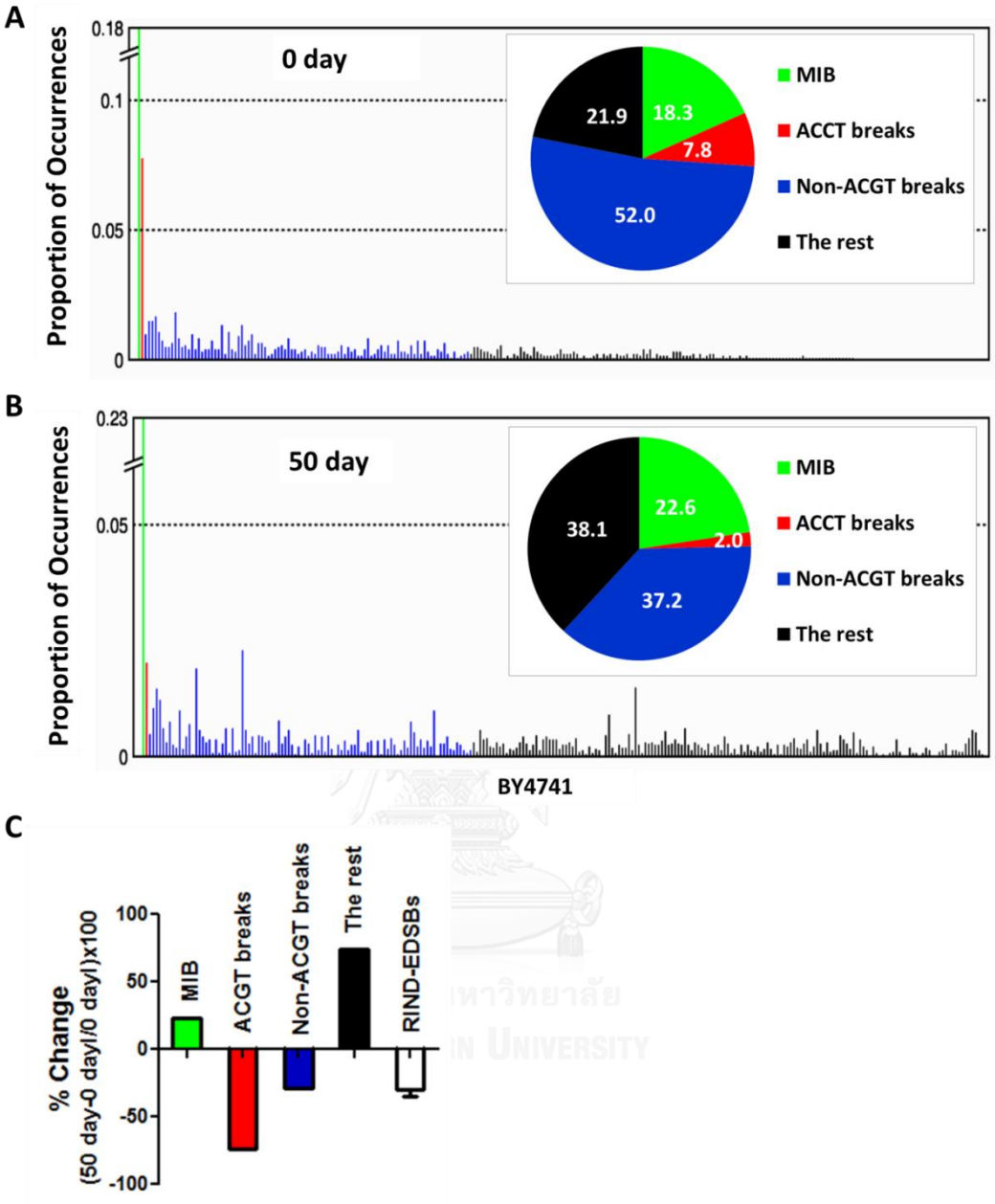

Figure 22 RIND-EDSBs and sequences in chronologically aging yeast. RIND-EDSB sequences based on 4 nucleotides located upstream to the break were classified into 4 types based on wild type day 0: (1) ACGT (ACGT breaks; red), (2) Non-ACGT breaks (blue), the 4 bp that was found more frequently (odds ratio > 1), (3) The rest (black), the breaks containing 4 bp that were unlikely to be found(odds ratio <1), (4) MIB (Modified Insertion at the Break; green), RIND-EDSBs that 5' end sequence downstream to the break did not match with genomic sequence and considered as an inserted bases

before the breaks. Pattern and proportion of RIND-EDSB sequences in wild type strain at day 0 **(A)** and day 50 **(B)**. **(C)** The % changes of RIND-EDSB level (white) and sequences (MIB; green, ACGT break; red, Non-ACGT breaks; blue and The rest; black) of day 50 compared to 0 day.

DSB repair defect

Aging cells had an increased proportion of The rest breaks (Fig 22C). Therefore, it is possible that aging cells have DSB repair defect. First, we evaluated how RIND-EDSB patterns in cells that DSB repair was inhibited changed. Cells were treated by caffeine, and ATM/ATR-dependent DSB repair inhibitor, for 24 hours. When cells were treated with caffeine, an increase in RIND-EDSB levels and a decrease in viability were observed (Dr. Jirapan, unpublished data). Among the four classes of RIND-EDSBs, a percentage of MIB and The rest number increased (Figure 23A, 23B and 23C). Therefore, caffeine treatment increased MIB and The rest. Interestingly, the % changes of RIND-EDSB patterns of caffeine treatment (Figure 23C) were similar to RIND-EDSB patterns of aging cells (Figure 22C). Therefore, we hypothesized that chronological aging cells lost DSB repair function.

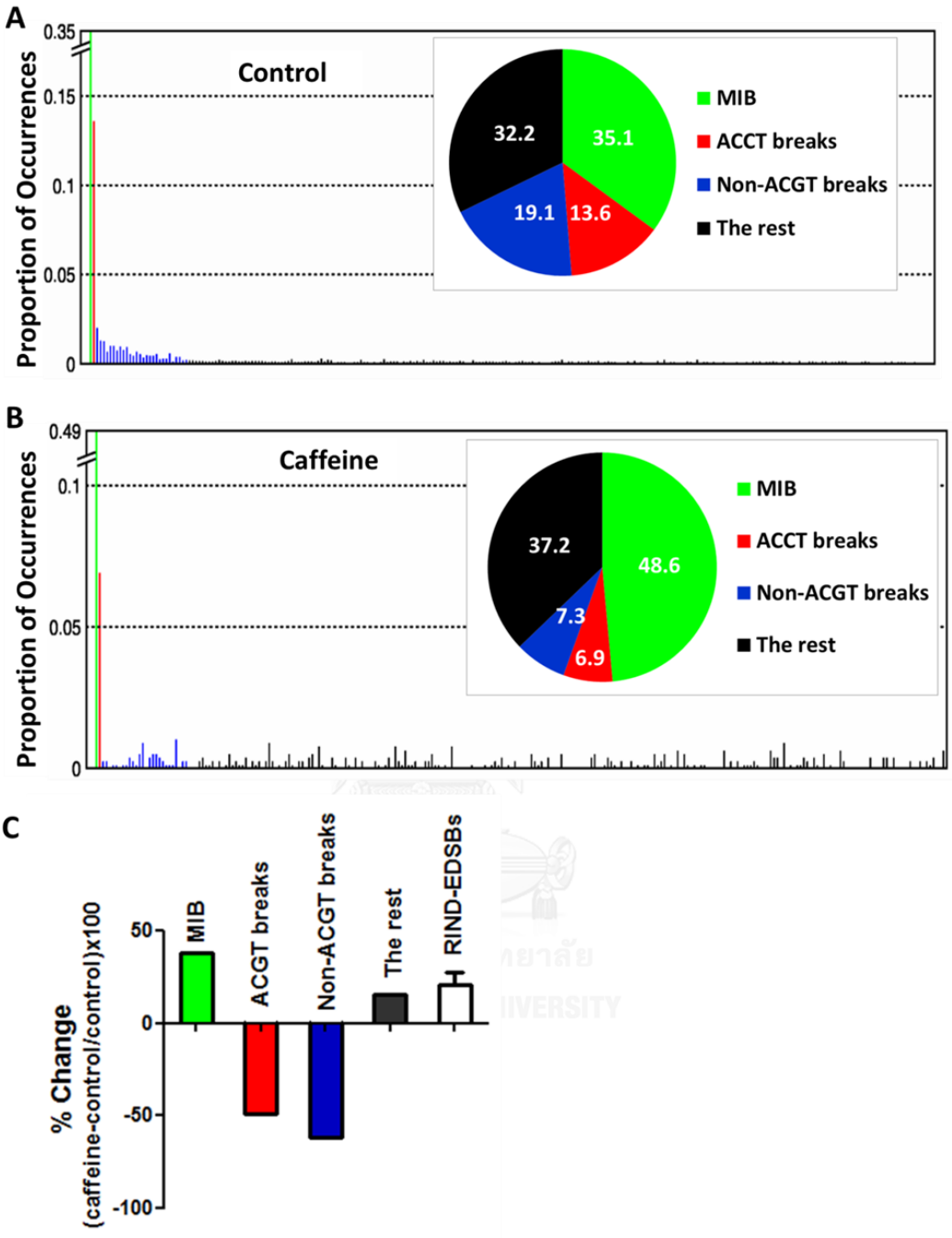
A
Control
Proportion of Occurrences
0.35
0.15
0.1
0.05
0
32.2
35.1
19.1
13.6
MIB
ACCT breaks
Non-ACGT breaks
The rest
B
Caffeine
Proportion of Occurrences
0.49
0.1
0.05
0
37.2
48.6
7.3
6.9
MIB
ACCT breaks
Non-ACGT breaks
The rest
C
% Change
(caffeine-control/control)x100
50
0
-50
-100
MIB
ACGT breaks
Non-ACGT breaks
The rest
RIND-EDSBs

Figure 23 sequence of caffeine treatment in JKM179 yeast strains. **(A)** Pattern and proportion of RIND-EDSB sequences in control (JKM179). **(B)** Pattern and proportion of RIND-EDSB sequences in caffeine (JKM179 with caffeine treatment). RIND-EDSB sequences based on 4 nucleotides located upstream to the break were classified into 4 types as in Figure 1 but OR were based on JKM179. **(C)** The % changes of RIND-EDSB level (white) and sequences (MIB; green, ACGT break; red, Non-ACGT breaks; blue and The rest; black) of JKM179 with caffeine treatment compared to control (JKM179).

DSB repair defect in chronological aging yeast

To prove the hypothesis that chronological aging cells lost DSB repair function, we induced a break every ten days in old culture of JKM179 by HO induction and observed whether cells could repair the break by measuring viability. We found significant reductions in viability in HO-induced yeast cells by days 20 and 30 (Figure 24) (p-value < 0.05 and 0.0001, respectively). Hence, aging cells lost DSB repair function.

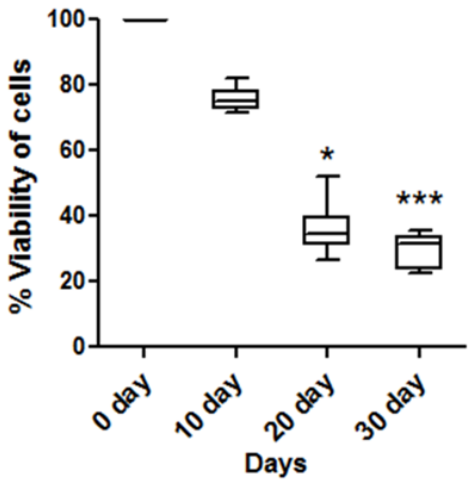

Figure 24 Percent viability on days 0-30 following HO induction. A break was induced every ten days in old culture of JKM179 by HO induction.

HO induction to reduce RIND-EDSBs

JKM179 was a yeast strain that carries galactose-inducible HO endonuclease (HO) and a specific irreparable HO specific site at the MAT locus with a deletion of homologous sequence at HML and HMR loci. The galactose-induced DSB cannot be repaired by the process of homologous recombination. The induction of HO endonuclease generates a single DSB and cells immediately try to repair the break. Previous experiment, we found that aging cells possessed low RIND-EDSB levels. Therefore, to support the study in chronological aging we set up the set of experiments in JKM197 yeast strain that showed the expression of HO endonuclease let to RIND-EDSB reduction.

Patterns of RIND-EDSB sequences in JKM179 strain were similar to wild type, in which ACGT breaks were also the most commonly found (Figure 25A). After HO induction, percentages of ACGT, Non-ACGT and The rest breaks were reduced (Figure 25B). Thus, HO induction decreased ACGT, Non-ACGT and The rest breaks (Figure 25C).

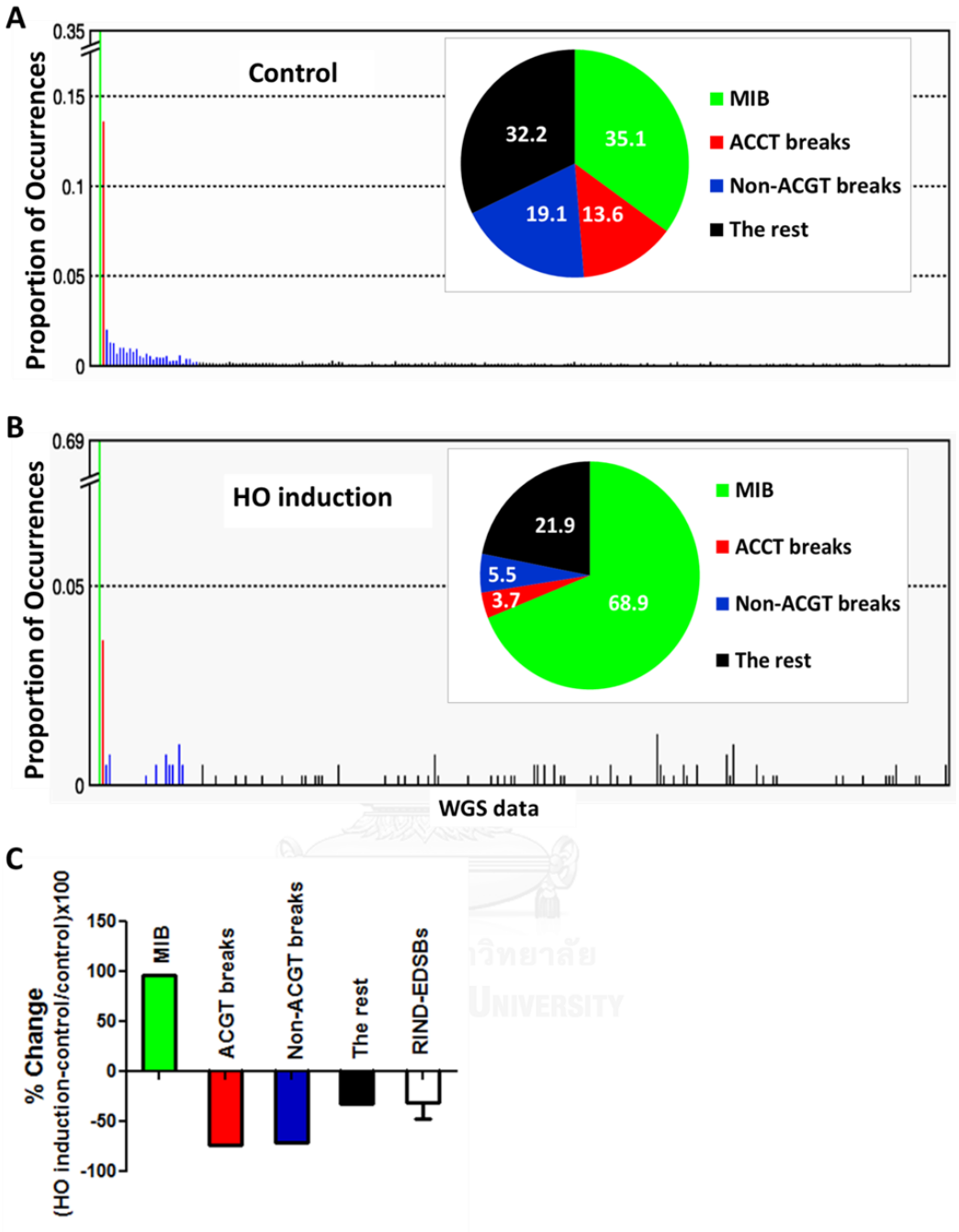

Figure 25 RIND-EDSBs and sequences in HO induction. Pattern and proportion of RIND-EDSB sequences in control (JKM179) **(A)** and HO induction (JKM179 with HO expression) **(B)**. **(C)** The %changes of RIND-EDSB level (white) and sequences (MIB; green, ACGT break; red, Non-ACGT breaks; blue and The rest; black) of HO induction compared to control (the same image as in the previous figure 23A).

What happened when cells containing low RIND-EDSBs had DSB repair defect?

Since both RIND-EDSB reduction and DSB repair defect were found in chronological aging cells, it is interesting to evaluate cells with low RIND-EDSBs together with DSB repair defect. Therefore, we treated HO induced cells with caffeine. We found that caffeine treatment to HO induced cells reduced cell viability (Dr. Jirapan, unpublished data) and increased RIND-EDSB levels, particularly non-ACGT and The rest breaks (Figure 26B), more than HO induced cells (Figure 26A) or caffeine treatment to non-induced cells (Figure 23B). Interestingly, while the proportion of ACGT breaks were reduced down to 0.9% (Figure 26B), overall RIND-EDSB levels were increased to 100% (white bar in Figure. 26C). This number clearly contrasts to a number in caffeine treatment to non-induced cells, in which overall RIND-EDSB levels were increased to only around 20% (white bar Figure 23C).

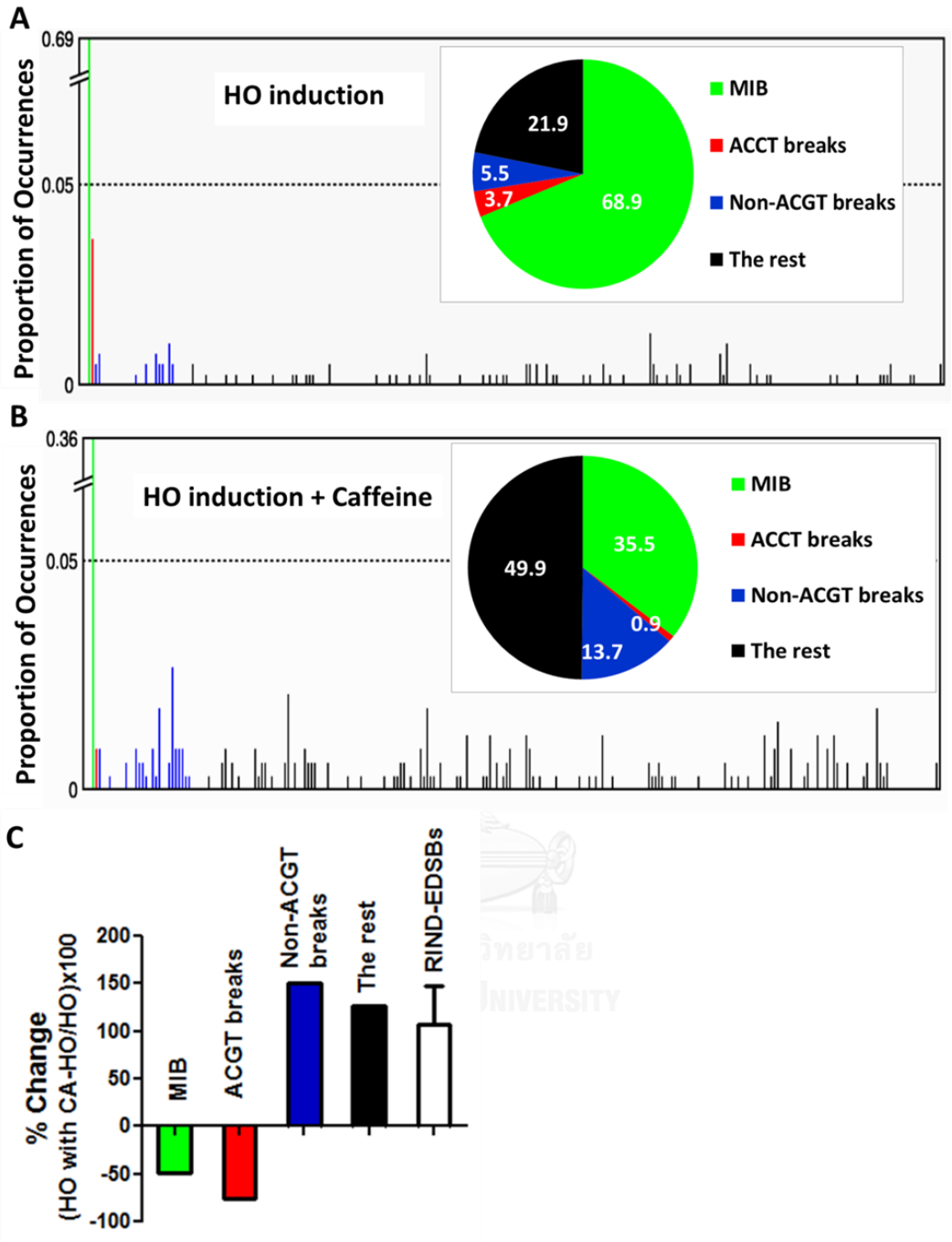

Figure 26 Sequence of caffeine treatment in HO induction. **(A)** Pattern and proportion of RIND-EDSB sequences in HO induction. **(B)** Pattern and proportion of RIND-EDSB sequences in HO induction plus caffeine. RIND-EDSB sequences based on 4 nucleotides located upstream to the break were classified into 4 types as in Figure 1 but OR were based on JKM179 **(C)** The % changes of RIND-EDSB patterns of HO induction plus caffeine compared to HO induction(the same image as in the previous figure 25B).

Our previous study showed that the mutant strain, *nhp6aΔ,* had a lower number of RIND-EDSBs (Dr. Jirapan, unpublished data). We therefore used *nhp6aΔ* as a low level RIND-EDSBs strain. Once, we treated *nhp6aΔ* with caffeine, similar changes in viability and EDSBs (Figure 26) to HO induced cells treated with caffeine were observed (Figure 25). Caffeine treatment increased RIND-EDSB, and also reduced viability (data not show). RIND-EDSB pattern of *nhp6aΔ* was similar to the others in that ACGT breaks were the most frequent (Figure 26A). Caffeine treatment to *nhp6aΔ* also altered the proportion of each break type and level of RIND-EDSBs was similar to caffeine treatment to HO induced cells (Figure 25A and 25B), in which new RIND-EDSBs were distributed in the genome widely, regardless of 4 base pair sequences prior to the breaks (Figure 26B). Finally, caffeine treatment to *nhp6aΔ* greatly reduced the proportion of ACGT break to 1.1% (Figure 26B) but increased the overall RIND-EDSB level to 115% (Figure 26C).

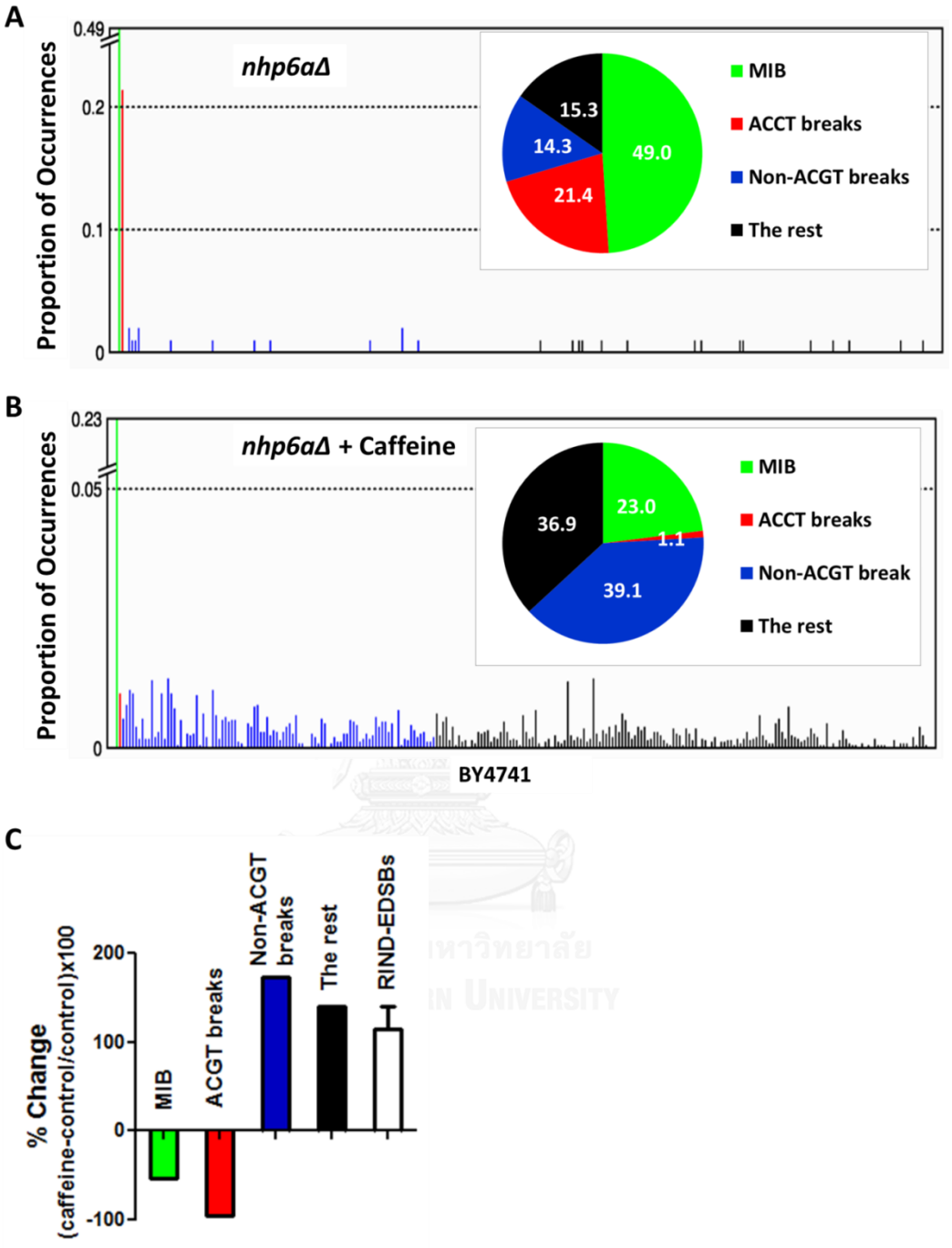

Figure 27 Sequence of nhp6a deletion yeast strains (*nhp6aΔ*). Pattern and proportion of RIND-EDSB sequences in *nhp6aΔ* **(A)** and *nhp6aΔ* plus caffeine (*nhp6aΔ* with caffeine treatment) **(B)**. RIND-EDSB sequences based on 4 nucleotides located upstream to the break were classified into 4 types as in Figure 1 but OR were based on wild type day 0. **(C)** The % changes of RIND-EDSB level (white) and sequences (MIB; green, ACGT

break; red, Non-ACGT breaks; blue and The rest; black) of *nhp6aΔ* plus caffeine compared to *nhp6aΔ*.

CHAPTER V
DISCUSSION

In this study, we aimed to study the epigenetic marks involve in genomic instability, a common event in aging. We focused on two epigenetic marks. First, it is methylation of Alu element, commonly studied IRS which was proposed to associate with aging characters. Second, it is endogenous DNA double strand breaks (EDSBs), which one of the genomic instability mechanisms in non-dividing cells, change in homeostasis during aging.

siRNA-Alu can increased Alu methylation level and play a role in DNA damage prevention

One of the most prevalent effects of intersperse repetitive sequence (IRS) hypomethylation is genomic instability, an imbalance of formation and repair of DNA damage, leads to accumulation of mutation within genome and commonly promotes aging (*59, 60*). Therefore, a tool to increase methylation of IRS would be useful to prevent genomic instability, a common precursor of aging and cancer. siRNA has been demonstrated de novo methylation (*13, 37, 38, 61*). Therefore, siRNA may be used as a tool to increase IRS methylation. Alu element, the human short interspersed elements, is commonly studied IRS. Moreover, Alu hypomethylation was found correlated to many aging conditions.

First, we discovered a strong negative liner correlation between Alu methylation in peripheral blood cells and endogenous DNA damage levels (8-OHdG and AP site) (Figure 12). The results suggested that Alu methylation in white blood cells of healthy people determine endogenous DNA damage lesions. Next, we evaluated whether siRNA-Alu can increase Alu methylation level. Therefore, siRNA-Alu was transfected to non-cancerous HEK293 cells, cancerous HeLa cells and PDL fibroblasts. We observed an increase in the level of Alu methylation in all cell types (Figure 13 and 18). Moreover, the methylation was sustainable because transfected HEK293 also resulted in an

increase in Alu methylation level after continuing cell culture for 7 days (Figure 16).The de novo methylation was sequence specific because there was no change in LINE-1 methylation level (Figure 15).

To prove whether increasing Alu methylation resulted from the binding of siRNA-Alu to Alu elements, Bisulfite Alu PCR amplicons were analyzed using high-throughput sequencing and compared methylation levels between siRNA-Alu transfected and control cells. The results showed that Alu methylation was more significant difference at 0.005 at certain position with higher %ID and indel was absent in the alignment (Figure 17). This result concluded that increasing level of Alu methylation induced by siRNA-Alu depended on siRNA binding sites having insertion or deletion (INDEL) and percent identity value.

Because of in young people, Alu methylation is directly associated with growth rate (*62*). Moreover, Alu methylation also reported to correlate with aging phenotypes such as osteoporosis (*12*), we therefore investigated whether increasing Alu methylation can change phenotypes of cells. First by assessment of cell proliferation using MTT and cell count assay, we found a significantly increased rate of proliferation in siRNA-Alu transfected cells in both HEK293 and PDL (Figure 19). So, we stated that Alu methylation altered cellular phenotypes. Hypermethylated Alu cells proliferated faster than control cells.

Next, we explored why hypermethylated Alu cells proliferated faster. In cell division, there are cell cycle controls or checkpoints in order to ensure proper division of the cell. Whenever damages were detected, cells can arrest until defects are repaired. For this reason, we hypothesized that Alu hypermethylation would reduce DNA damages therefore cells could push normal progression through cell cycle. To prove this hypothesis, control and siRNA-Alu transfected cells with significantly increasing Alu methylation were exposed to DNA damage agent. Exposure of HEK293 and PDL cells to MMS and H_2O_2 showed that %cell survival of hypermethylated Alu cells was significant higher than control cells (Figure 20).Our results can conclude that Alu hypermethylated

cells increased resistance to DNA damage agent. To increase confident in this hypothesis, we monitored the level of endogenous DNA damages (8-OHdG and AP site). Lower level of 8-OHdG and AP site was observed in Alu hypermethylated cells (Figure 21).

Here, we demonstrated that siRNA-Alu can increase Alu methylation level and may play a role in prevent genomic instability by reducing DNA damages and increasing resistance to DNA damaging agents. siRNA-Alu would be useful tool to investigate the underlining mechanism of how DNA methylation prevents DNA lesions. Global hypomethylation, which generates genomic instability, is a prevalent molecular event in cancer and aging. Thus, siRNA-Alu promoting Alu methylation technology has high potential to inhibit genomic instability in cancer and the aging process in the future.

Endogenous DNA double-strand break sequences define genomic instability mechanism in aging of non-dividing yeast

Under normal physiologic condition, ACGT and Non-ACGT breaks are RIND-EDSBs that are retained in cells and possess physiologic function, phy-RIND-EDSBs. In chronological aging, the phy-RIND-EDSBs reduction and DSB repair defect result in pathologic DNA lesion, path-RIND-EDSBs retention and reduction of viability.

ACGT and Non-ACGT breaks are phy-RIND-EDSBs. Phy-RIND-EDSBs may play a role in reducing DNA tension and preventing path-RIND-EDSBs. Our previous results showed that RIND-EDSBs increased under caffeine treatment, which inhibits DSB repair, particularly at The rest break locations. Therefore, a type of RIND-EDSBs are spontaneously produced but immediately repaired. These RIND-EDSBs that were only found under DSB repair defect condition have similar roles as DSB occurred under pathologic conditions, path-RIND-EDSBs. A production of path-RIND-EDSB observed in low level ACGT and Non-ACGT breaks cells treated with caffeine treatment i.e., HO induced or cells lacking *nhp6aΔ*, were four times greater than normal cells. This

confirmed that phy-RIND-EDSBs play a role in reducing DNA stress and consequently prevent a spontaneous path-RIND-EDSBs production.

There may be several underlining mechanisms that generate low RIND-EDSB levels in aging yeast. In human, we found that RIND-EDSB levels were low when cells were treated with Trichostatin A, histone deacetylase inhibitor (*16*). Yeast lacking one of the HMG genes or *SIR2* also contained low RIND-EDSB levels (*56*). In this study, we showed that induction of a DSB could induce genome wide EDSB repair and consequently reduced RIND-EDSBs. Moreover, we found that new path-RIND-EDSBs can spontaneously be occurred. Therefore, it is possible that these path-RIND-EDSBs globally induced the retained phy-RIND-EDSB repair. Consequently, we found ACGT and Non-ACGT breaks reduction in chronological aging yeast.

Caffeine treatment also increased MIB breaks. There were several enzymatic mechanisms that were reported to insert extra bases to a DNA strand similar to MIB including terminal transferase activity, non-homologous end joining and action of reverse transcriptase (*63-65*). Because MIBs were increased by caffeine treatment, we hypothesized that MIB is end modification by an alternate DSB repair pathway.

Here, we also proved that chronological aging yeast had DSB repair defect. First, we found that both aging yeast and caffeine treated cells had an increased proportion of The rest and MIB breaks. That is aging yeast had similar RIND-EDSB patterns to cells treated with DSB repair inhibitor. Moreover, we found that the more cells aged, the lower the number of cells survived an induction of a DSB. Therefore, aging yeast lost a capability in repairing DSBs.

Path-RIND-EDSBs can send senescence signals. It is known that DSBs promote H2AX and H2AX sends senescence signals to cells (*48, 49*). Here, we found that a combination of reduction of phy-RIND-EDSBs and DSB repair defect caused path-RIND-EDSB retention. Because this combination is found in aging cells, it is reasonable to

hypothesize that path-RIND-EDSB retention is a key for senescence signalling in the chronological aging process.

In conclusion, under normal condition phy-RIND-EDSBs are retained to reduce DNA tension. Spontaneous occurrence of path-RIND-EDSBs can induce genome-wide RIND-EDSB repair. Consequently, phy-RIND-EDSBs are reduced in chronological aging cells. Low phy-RIND-EDSB cells have high DNA tension and produce a high number of new path-RIND-EDSBs. Together with DSB repair defect in aging cells, path-RIND-EDSBs are retained in aging cells and consequently promote cellular senescence (Figure 28).

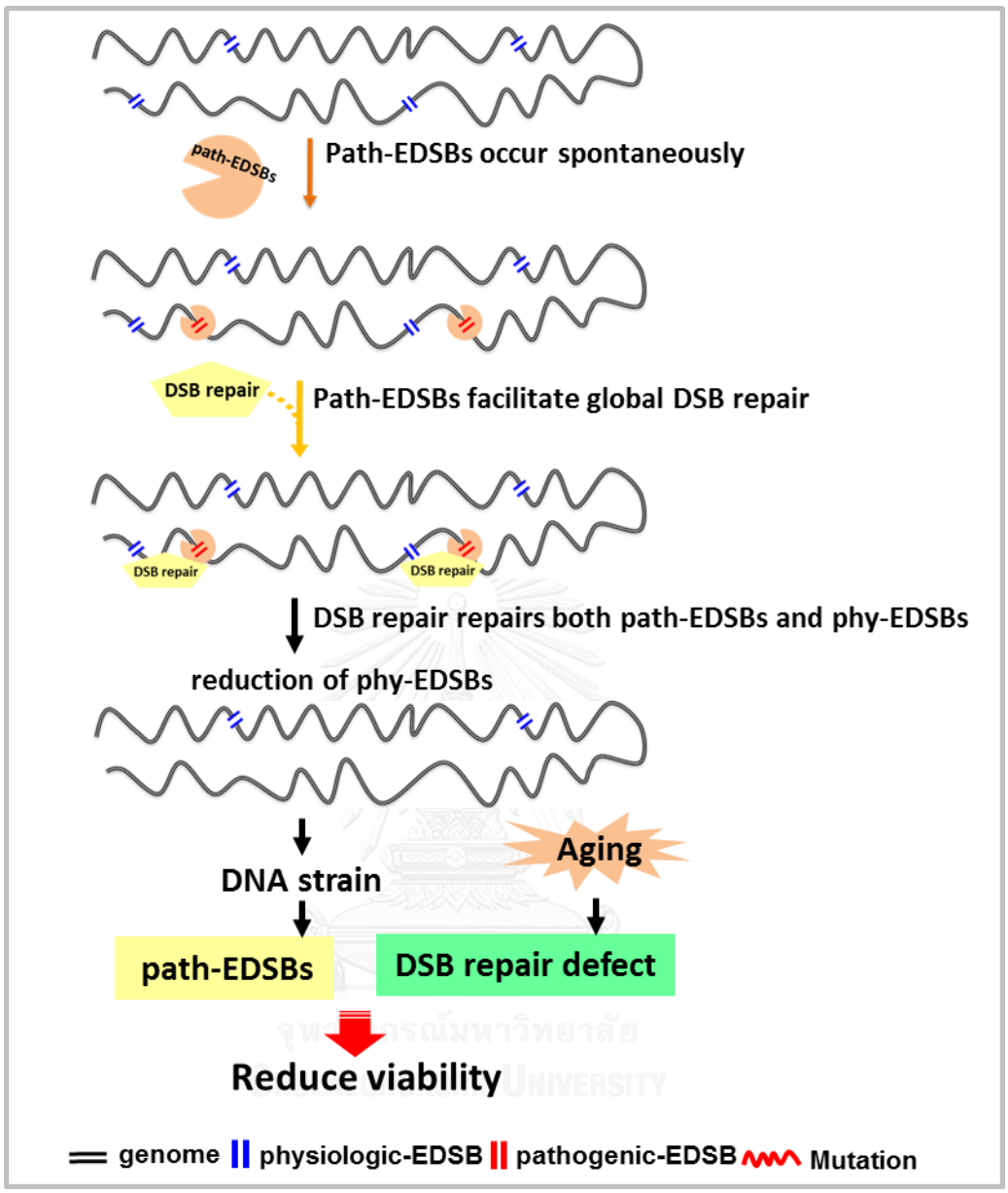

Figure 28 Schematic representation of how RIND-EDSBs reduce cell viability during the yeast life cycle.

REFERENCES

1. C. J. Lord, A. Ashworth, The DNA damage response and cancer therapy. *Nature* **481**, 287-294 (2012).
2. A. A. Moskalev, M. V. Shaposhnikov, E. N. Plyusnina, A. Zhavoronkov, A. Budovsky, H. Yanai, V. E. Fraifeld, The role of DNA damage and repair in aging through the prism of Koch-like criteria. *Ageing research reviews* **12**, 661-684 (2013).
3. A. Tubbs, A. Nussenzweig, Endogenous DNA damage as a source of genomic instability in cancer. *Cell* **168**, 644-656 (2017).
4. W. Barbot, A. Dupressoir, V. Lazar, T. Heidmann, Epigenetic regulation of an IAP retrotransposon in the aging mouse: progressive demethylation and de-silencing of the element by its repetitive induction. *Nucleic acids research* **30**, 2365-2373 (2002).
5. P. J. Hornsby, L. Yang, L. E. Gunter, Demethylation of satellite I DNA during senescence of bovine adrenocortical cells in culture. *Mutation Research/DNAging* **275**, 13-19 (1992).
6. L. Mays-Hoopes, A. Brown, R. Huang, Methylation and rearrangement of mouse intracisternal a particle genes in development, aging, and myeloma. *Molecular and cellular biology* **3**, 1371-1380 (1983).
7. T. Ono, K. Shinya, Y. Uehara, S. Okada, Endogenous virus genomes become hypomethylated tissue—specifically during aging process of C57BL mice. *Mechanisms of ageing and development* **50**, 27-36 (1989).
8. R. E. Mills, E. A. Bennett, R. C. Iskow, S. E. Devine, Which transposable elements are active in the human genome? *Trends in genetics* **23**, 183-191 (2007).
9. M. Pheasant, J. S. Mattick, Raising the estimate of functional human sequences. *Genome research* **17**, 1245-1253 (2007).
10. V. Bollati, J. Schwartz, R. Wright, A. Litonjua, L. Tarantini, H. Suh, D. Sparrow, P. Vokonas, A. Baccarelli, Decline in genomic DNA methylation through aging in a

cohort of elderly subjects. *Mechanisms of ageing and development* **130**, 234-239 (2009).

11. P. Jintaridth, A. Mutirangura, Distinctive patterns of age-dependent hypomethylation in interspersed repetitive sequences. *Physiological genomics* **41**, 194-200 (2010).
12. P. Jintaridth, R. Tungtrongchitr, S. Preutthipan, A. Mutirangura, Hypomethylation of Alu elements in post-menopausal women with osteoporosis. *PLoS One* **8**, e70386 (2013).
13. D. Castanotto, S. Tommasi, M. Li, H. Li, S. Yanow, G. P. Pfeifer, J. J. Rossi, Short hairpin RNA-directed cytosine (CpG) methylation of the RASSF1A gene promoter in HeLa cells. *Molecular Therapy* **12**, 179-183 (2005).
14. H. Kawasaki, K. Taira, Induction of DNA methylation and gene silencing by short interfering RNAs in human cells. *Nature* **431**, 211-217 (2004).
15. M. Lomax, L. Folkes, P. O'Neill, Biological consequences of radiation-induced DNA damage: relevance to radiotherapy. *Clinical oncology* **25**, 578-585 (2013).
16. N. Kongruttanachok, C. Phuangphairoj, A. Thongnak, W. Ponyeam, P. Rattanatanyong, W. Pornthanakasem, A. Mutirangura, Replication independent DNA double-strand break retention may prevent genomic instability. *Molecular cancer* **9**, 70 (2010).
17. J. Seo, S. C. Kim, H.-S. Lee, J. K. Kim, H. J. Shon, N. L. M. Salleh, K. V. Desai, J. H. Lee, E.-S. Kang, J. S. Kim, Genome-wide profiles of H2AX and γ-H2AX differentiate endogenous and exogenous DNA damage hotspots in human cells. *Nucleic acids research*, gks287 (2012).
18. W. Pornthanakasem, N. Kongruttanachok, C. Phuangphairoj, C. Suyarnsestakorn, T. Sanghangthum, S. Oonsiri, W. Ponyeam, T. Thanasupawat, O. Matangkasombut, A. Mutirangura, LINE-1 methylation status of endogenous DNA double-strand breaks. *Nucleic acids research* **36**, 3667-3675 (2008).

19. M. Pongpanich, M. Patchsung, J. Thongsroy, A. Mutirangura, Characteristics of replication-independent endogenous double-strand breaks in Saccharomyces cerevisiae. *BMC genomics* **15**, 750 (2014).

20. M. A. Batzer, P. L. Deininger, Alu repeats and human genomic diversity. *Nature reviews genetics* **3**, 370-379 (2002).

21. P. L. Deininger, J. V. Moran, M. A. Batzer, H. H. Kazazian, Mobile elements and mammalian genome evolution. *Current opinion in genetics & development* **13**, 651-658 (2003).

22. K. Chalitchagorn, S. Shuangshoti, N. Hourpai, N. Kongruttanachok, P. Tangkijvanich, D. Thong-ngam, N. Voravud, V. Sriuranpong, A. Mutirangura, Distinctive pattern of LINE-1 methylation level in normal tissues and the association with carcinogenesis. *Oncogene* **23**, 8841-8846 (2004).

23. P. Sirivanichsuntorn, S. Keelawat, K. Danuthai, A. Mutirangura, K. Subbalekha, N. Kitkumthorn, LINE-1 and Alu hypomethylation in mucoepidermoid carcinoma. *BMC clinical pathology* **13**, 10 (2013).

24. D. Tiwawech, R. Srisuttee, P. Rattanatanyong, C. Puttipanyalears, N. Kitkumthorn, A. Mutirangura, Alu methylation in serum from patients with nasopharyngeal carcinoma. *Asian Pac J Cancer Prev* **15**, 9797-9800 (2014).

25. C. Puttipanyalears, K. Subbalekha, A. Mutirangura, N. Kitkumthorn, Alu hypomethylation in smoke-exposed epithelia and oral squamous carcinoma. *Asian Pacific Journal of Cancer Prevention* **14**, 5495-5501 (2013).

26. J. H. Hoeijmakers, Genome maintenance mechanisms for preventing cancer. *nature* **411**, 366-374 (2001).

27. L. Lavie, M. Kitova, E. Maldener, E. Meese, J. Mayer, CpG methylation directly regulates transcriptional activity of the human endogenous retrovirus family HERV-K (HML-2). *Journal of virology* **79**, 876-883 (2005).

28. J. Nakkuntod, P. Sukkapan, Y. Avihingsanon, A. Mutirangura, N. Hirankarn, DNA methylation of human endogenous retrovirus in systemic lupus erythematosus. *Journal of human genetics* **58**, 241-249 (2013).

29. P. Tongyoo, Y. Avihingsanon, S. Prom-On, A. Mutirangura, W. Mhuantong, N. Hirankarn, EnHERV: Enrichment analysis of specific human endogenous retrovirus patterns and their neighboring genes. *PloS one* **12**, e0177119 (2017).

30. C. López-Otín, M. A. Blasco, L. Partridge, M. Serrano, G. Kroemer, The hallmarks of aging. *Cell* **153**, 1194-1217 (2013).

31. E. S. Lander, L. M. Linton, B. Birren, C. Nusbaum, M. C. Zody, J. Baldwin, K. Devon, K. Dewar, M. Doyle, W. FitzHugh, Initial sequencing and analysis of the human genome. *Nature* **409**, 860-921 (2001).

32. M. Dewannieux, C. Esnault, T. Heidmann, LINE-mediated retrotransposition of marked Alu sequences. *Nature genetics* **35**, 41-48 (2003).

33. M. R. Paule, R. J. White, Survey and summary transcription by RNA polymerases I and III. *Nucleic acids research* **28**, 1283-1298 (2000).

34. C. Mugatroyd, Y. Wu, Y. Bockmühl, D. Spengler, The Janus face of DNA methylation in aging. *Aging (Albany NY)* **2**, 107-110 (2010).

35. R. K. Slotkin, R. Martienssen, Transposable elements and the epigenetic regulation of the genome. *Nature Reviews Genetics* **8**, 272-285 (2007).

36. M. Wassenegger, RNA-directed DNA methylation. *Plant molecular biology* **43**, 203-220 (2000).

37. A. Hamilton, O. Voinnet, L. Chappell, D. Baulcombe, Two classes of short interfering RNA in RNA silencing. *The EMBO journal* **21**, 4671-4679 (2002).

38. S. W.-L. Chan, D. Zilberman, Z. Xie, L. K. Johansen, J. C. Carrington, S. E. Jacobsen, RNA silencing genes control de novo DNA methylation. *Science* **303**, 1336-1336 (2004).

39. V. D. Longo, G. S. Shadel, M. Kaeberlein, B. Kennedy, Replicative and chronological aging in Saccharomyces cerevisiae. *Cell metabolism* **16**, 18-31 (2012).

40. P. Fabrizio, V. D. Longo, The chronological life span of Saccharomyces cerevisiae. *Aging cell* **2**, 73-81 (2003).

41. P. Fabrizio, V. D. Longo, The chronological life span of Saccharomyces cerevisiae. *Biological Aging: Methods and Protocols*, 89-95 (2007).

42. P. Fabrizio, F. Pozza, S. D. Pletcher, C. M. Gendron, V. D. Longo, Regulation of longevity and stress resistance by Sch9 in yeast. *Science* **292**, 288-290 (2001).

43. P. Fabrizio, L. Battistella, R. Vardavas, C. Gattazzo, L.-L. Liou, A. Diaspro, J. W. Dossen, E. B. Gralla, V. D. Longo, Superoxide is a mediator of an altruistic aging program in Saccharomyces cerevisiae. *The Journal of cell biology* **166**, 1055-1067 (2004).

44. F. Madia, C. Gattazzo, M. Wei, P. Fabrizio, W. C. Burhans, M. Weinberger, A. Galbani, J. R. Smith, C. Nguyen, S. Huey, Longevity mutation in SCH9 prevents recombination errors and premature genomic instability in a Werner/Bloom model system. *The Journal of cell biology* **180**, 67-81 (2008).

45. F. Madia, M. Wei, V. Yuan, J. Hu, C. Gattazzo, P. Pham, M. F. Goodman, V. D. Longo, Oncogene homologue Sch9 promotes age-dependent mutations by a superoxide and Rev1/Polζ-dependent mechanism. *The Journal of cell biology* **186**, 509-523 (2009).

46. F. Madia, C. Gattazzo, P. Fabrizio, V. D. Longo, A simple model system for age-dependent DNA damage and cancer. *Mechanisms of ageing and development* **128**, 45-49 (2007).

47. V. D. Longo, P. Fabrizio, in *Aging Research in Yeast*. (Springer, 2011), pp. 101-121.

48. M. Löbrich, A. Shibata, A. Beucher, A. Fisher, M. Ensminger, A. A. Goodarzi, O. Barton, P. A. Jeggo, γH2AX foci analysis for monitoring DNA double-strand break repair: strengths, limitations and optimization. *Cell cycle* **9**, 662-669 (2010).

49. I. Revet, L. Feeney, S. Bruguera, W. Wilson, T. K. Dong, D. H. Oh, D. Dankort, J. E. Cleaver, Functional relevance of the histone γH2Ax in the response to DNA damaging agents. *Proceedings of the National Academy of Sciences* **108**, 8663-8667 (2011).

50. M. M. Vilenchik, A. G. Knudson, Endogenous DNA double-strand breaks: production, fidelity of repair, and induction of cancer. *Proceedings of the National Academy of Sciences* **100**, 12871-12876 (2003).

51. Y. Aylon, M. Kupiec, DSB repair: the yeast paradigm. *DNA repair* **3**, 797-815 (2004).

52. J. Ringvoll, L. M. Nordstrand, C. B. Vågbø, V. Talstad, K. Reite, P. A. Aas, K. H. Lauritzen, N. B. Liabakk, A. Bjørk, R. W. Doughty, Repair deficient mice reveal mABH2 as the primary oxidative demethylase for repairing 1meA and 3meC lesions in DNA. *The EMBO journal* **25**, 2189-2198 (2006).

53. S. M. Phipps, J. B. Berletch, L. G. Andrews, T. O. Tollefsbol, Aging Cell Culture. *Biological Aging*, 9.

54. S. Dango, N. Mosammaparast, M. E. Sowa, L.-J. Xiong, F. Wu, K. Park, M. Rubin, S. Gygi, J. W. Harper, Y. Shi, DNA unwinding by ASCC3 helicase is coupled to ALKBH3-dependent DNA alkylation repair and cancer cell proliferation. *Molecular cell* **44**, 373-384 (2011).

55. P. F. Larrosa, M. R. Grecco, D. M. Gómez, C. Alvarado, L. Panelo, M. Rubio, D. Alonso, D. Gómez, M. Costas, RAC3 more than a nuclear receptor coactivator: a key inhibitor of senescence that is downregulated in aging. *Cell death & disease* **6**, e1902 (2015).

56. J. Thongsroy, O. Matangkasombut, A. Thongnak, P. Rattanatanyong, S. Jirawatnotai, A. Mutirangura, Replication-independent endogenous DNA double-strand breaks in Saccharomyces cerevisiae model. *PloS one* **8**, e72706 (2013).

57. B. A. Moser, J.-M. Brondello, B. Baber-Furnari, P. Russell, Mechanism of caffeine-induced checkpoint override in fission yeast. *Molecular and cellular biology* **20**, 4288-4294 (2000).

58. J.-A. Kim, M. Kruhlak, F. Dotiwala, A. Nussenzweig, J. E. Haber, Heterochromatin is refractory to γ-H2AX modification in yeast and mammals. *The Journal of cell biology* **178**, 209-218 (2007).

59. R. Z. Chen, U. Pettersson, C. Beard, L. Jackson-Grusby, R. Jaenisch, DNA hypomethylation leads to elevated mutation rates. *Nature* **395**, 89-93 (1998).

60. F. Gaudet, J. G. Hodgson, A. Eden, L. Jackson-Grusby, J. Dausman, J. W. Gray, H. Leonhardt, R. Jaenisch, Induction of tumors in mice by genomic hypomethylation. *Science* **300**, 489-492 (2003).

61. M. Mette, W. Aufsatz, J. Van der Winden, M. Matzke, A. Matzke, Transcriptional silencing and promoter methylation triggered by double-stranded RNA. *The EMBO journal* **19**, 5194-5201 (2000).

62. K. Rerkasem, P. Rattanatanyong, A. Rerkasem, A. Wongthanee, K. Rungruengthanakit, A. Mangklabruks, A. Mutirangura, Higher Alu methylation levels in catch-up growth in twenty-year-old offsprings. *PloS one* **10**, e0120032 (2015).

63. A. Bianchi, S. Negrini, D. Shore, Delivery of yeast telomerase to a DNA break depends on the recruitment functions of Cdc13 and Est1. *Molecular cell* **16**, 139-146 (2004).

64. M. L. Hefferin, A. E. Tomkinson, Mechanism of DNA double-strand break repair by non-homologous end joining. *DNA repair* **4**, 639-648 (2005).

65. S.-C. Teng, B. Kim, A. Gabriel, Retrotransposon reverse-transcriptase-mediated repair of chromosomal breaks. *Nature* **383**, 641 (1996).

APPENDIX

VITA

Miss Maturada Patchsung was born on July 21, 1985 in Nontaburi, Thailand. She received her Bachelor degree of Science (B.Sc.) from Chulalongkorn University. In 2011, she graduated from Chulalongkorn University, Medicine Faculty with a master degree of Medical Biochemistry. Then, she has enrolled Chulongkorn University in graduate program for Docteral degree of Biomedical Science since 2012.